








## RESEARCH ARTICLE

# Characterizing Australia's east coast cyclones (1950–2019)

Jessie L. Gray<sup>1</sup>  | Danielle C. Verdon-Kidd<sup>2</sup>  | Jasmine B. D. Jaffrés<sup>3</sup>  |  
 Michael G. Hewson<sup>4</sup>  | John M. Clarke<sup>5</sup>  | Krishneel K. Sharma<sup>2,6</sup>  |  
 Nathan B. English<sup>1</sup> 

<sup>1</sup>School of Health, Medical and Applied Sciences, Central Queensland University, Townsville, Queensland, Australia

<sup>2</sup>School of Environmental and Life Sciences, University of Newcastle, Callaghan, New South Wales, Australia

<sup>3</sup>C&R Consulting, Townsville, Queensland, Australia

<sup>4</sup>School of Education and the Arts Central Queensland University, Rockhampton, Queensland, Australia

<sup>5</sup>CSIRO Climate Science Centre, Aspendale, Melbourne, Victoria, Australia

<sup>6</sup>Centre for New Energy Transition Research, Federation University, Mt Helen, Ballarat, Australia

**Correspondence**

Jessie L. Gray, School of Health, Medical and Applied Sciences, Central Queensland University, Townsville, Queensland 4810, Australia.

Email: [j.gray2@cqu.edu.au](mailto:j.gray2@cqu.edu.au)

**Funding information**

C&R Consulting, Townsville, Queensland 4814, Australia; Commonwealth Scientific and Industrial Research Organisation

**Abstract**

East coast cyclones (ECCs) provide an essential reprieve from dry periods across eastern Australia. They also deliver flood-producing rains with significant economic, social and environmental impacts. Assessing and comparing the influence of different types of cyclones is hindered by an incomplete understanding of ECC typology, given their widely variable spatial and temporal characteristics. This study employs a track-clustering method (probabilistic, curve-aligned regression model) to identify key cyclonic pathways for ECCs from 1950 to 2019. Six spatially independent clusters were successfully distinguished and further subclassified (coastal, continental and tropical) based on their genesis location. The seasonality and long-term variability, intensity (maximum Laplacian value  $\pm 2$  days) and event-based rainfall were then evaluated for each cluster to quantify the impact of these lows on Australia. The highest quantity of land-based rainfall per event is associated with the tropical cluster (Cluster 6), whereas widespread rainfall was also found to occur in the two continental clusters (clusters 4 and 5). Cyclone tracks orientated close to the coast (clusters 1, 2 and 3) were determined to be the least impactful in terms of rainfall and intensity, despite being the most common cyclone type. In terms of interannual variability, sea surface temperature anomalies suggest an increased cyclone frequency for clusters 1 (austral winter) and 4 (austral spring) during a central Pacific El Niño. Furthermore, cyclone incidence during IOD-negative conditions was more pronounced in winter for clusters 1, 2, 3— and clusters 4 and 5 in spring. All cyclones also predominantly occurred in SAM-positive conditions. However, winter ECCs for clusters 1 and 3 had a higher frequency in SAM-negative. This new typology of ECCs via spatial clustering provides crucial insights into the systems that produce extreme rainfall across eastern Australia and should be used to inform future hazard management of cyclone events.

**KEYWORDS**

Australia, east coast cyclones, eastern seaboard, ECL, ENSO, IOD, regression mixture model cluster analysis

This is an open access article under the terms of the [Creative Commons Attribution-NonCommercial-NoDerivs](https://creativecommons.org/licenses/by-nc-nd/4.0/) License, which permits use and distribution in any medium, provided the original work is properly cited, the use is non-commercial and no modifications or adaptations are made.

© 2023 The Authors. *International Journal of Climatology* published by John Wiley & Sons Ltd on behalf of Royal Meteorological Society.

## 1 | INTRODUCTION

East coast cyclones (ECCs) are the name given to storms that impact and occur along the eastern seaboard of Australia (Browning & Goodwin, 2013; Holland, 1997; Hopkins & Holland, 1997; McBride & Holland, 1987). ECC sub-categories outlined by Browning and Goodwin (2013, 2016) include easterly trough lows (ETLs), southern secondary lows (SSLs), inland trough lows (ITLs), continental lows (CLs) and extra-tropical cyclones (ETCs). All of these play a broad role in recharging freshwater systems and also cause extensive damage to communities along the east coast of Australia. Notable ECC events for Australia include the 1998 Sydney to Hobart Yacht Race (Buckley & Leslie, 2000; Greenslade, 2001; Mills, 2001) and the Pasha Bulker storm in June 2007 (Cavicchia et al., 2018; Verdon-Kidd et al., 2010, 2016). Both events were catastrophic: The 1998 Yacht Race resulted in the death of six people, the retirement of 71 yachts, the sinking of five yachts and the rescue of 55 crew by civil and military aircraft (the estimated cost was \$30 million; Australian Institute for Disaster Resilience, 2020; Greenslade, 2001; Mills, 2001). Conversely, the Pasha Bulker storm beached a 40,000-tonne bulk carrier ship on Nobby's Beach in Newcastle, New South Wales (NSW; Cavicchia et al., 2018; Verdon-Kidd et al., 2010, 2016), resulted in nine deaths, extensive flooding and wind damage to the Hunter region (resulting in a power loss for more than 300,000 people).

Australian ECC events can occur any time of the year but have been noted at higher frequency during the austral autumn and winter months (Browning & Goodwin, 2013; Speer et al., 2009; Verdon-Kidd et al., 2016)—or April–October (Kiem et al., 2016). The interannual variability of ECC events appears to be at least partially modulated by the state of large-scale climate modes that either inhibit or prime the localised environments required for storm development. Anomalous sea surface temperatures (SSTs) can be used as a proxy to infer the status of climate modes—such as the El Niño Southern Oscillation (ENSO) and the Indian Ocean Dipole (IOD)—that have subsequently been linked to driving the number of ECC events (Browning & Goodwin, 2013; Kiem et al., 2016; Speer et al., 2009; Verdon-Kidd et al., 2016). Increased storm numbers have been observed in La Niña years (Browning & Goodwin, 2013; Verdon-Kidd et al., 2016). Conversely, studies such as Dowdy, Mills, Timbal, and Wang (2013b); Dowdy et al. (2019) and Pepler, Coutts-Smith, and Timbal (2014); Pepler, Timbal, et al. (2014) have found a very weak relationship between ECC events and major climate drivers like ENSO as a result of data sensitivity and the dataset used. Transitional ENSO periods have also

been linked to enhanced storm genesis due to unstable offshore SSTs (Hopkins & Holland, 1997; Verdon-Kidd et al., 2016). The Southern Annular Mode (SAM) also influences conditions conducive to ECC events. Browning and Goodwin (2013) found periods of heightened ETL occurrences during weakly positive or neutral SAM. Furthermore, periods of enhanced storm activity have also been attributed to multi-modal climate signatures—for example, a neutral ENSO or the La Niña phase in the Pacific Ocean, combined with cool SST anomalies in the tropical Indian Ocean and neutral or positive SAM (Browning & Goodwin, 2013).

Although previous studies have explored the relationship of climate drivers with ECC events, they have typically been very limited in their temporal range (i.e. data ranging from 1970 onwards, with the exception of Browning & Goodwin, 2016 and Ji et al., 2018). This brevity of data has hindered definite correlations or tests of the long-term stability of observed teleconnections. Furthermore, many studies have also restricted the cyclone 'search radius' to just the eastern coastline. However, some of the most impactful cyclones (in terms of producing flooding rains) are known to have been continental or inland lows (e.g. the February 2020 east coast low [ECL] event; Mortlock & Somerville, 2020; PERILS, 2020). A recent comparative study of Australian ECL datasets confirmed that the NCEP1 database from Pepler (2020a, 2020b) has a more extensive spatial and temporal (1950–2019) track coverage (Gray et al., 2021) than other databases. Furthermore, Gray et al. (2021) highlighted the potential of NCEP1 to extend ECC climatology and research beyond the traditional boundaries commonly used in Australia. This provides a timely new opportunity to revisit ECCs, their impacts and their causal mechanisms over an extended time period and a broader geographical range.

Previous studies have clustered ECCs into distinct geographical groups to aid in the analysis and impact assessment. For example, spatial clustering has been applied to assess the synoptic type and group similar events for the eastern seaboard in Australia (Browning & Goodwin, 2013, 2016; Kiem et al., 2016). All three studies used the same three-stage-objective clustering algorithm (Browning & Goodwin, 2013), whereby closed lows are identified from the pressure gradient of 500 hPa on a 1.5° grid at 6-h intervals. The geographical location of the mean direction was constructed from the last data point to the beginning of the event. These studies grouped similar events based on their genesis location and orientation. As a result, they successfully identified more ECC events than in previous, subjective studies in Australia. However, this method focused on point data and did not assess or group by track characteristics. Previous studies

in Australia (Quinting, Reeder, & Catto, 2019b; Ramsay et al., 2012) have demonstrated how advantageous cluster analysis using tracks has been in investigating spatial and temporal trends of tropical cyclone (TC) events, a field of research that has not been applied in-depth for ECC events.

Many global studies (Corporal-Lodangco et al., 2014; Dacre & Pinto, 2020; Mailier et al., 2006; Mumby et al., 2011; Pinto et al., 2013; Quinting, Catto, & Reeder, 2019; Wolff et al., 2016; Yu et al., 2017) have demonstrated the effectiveness of cyclone clustering tools in forecasting and mitigating adverse storm effects and distinguishing impact-based approaches for risk and insurance management. Importantly, these methods can capture the path of the cyclone and the total spatiotemporal variability in the groupings. Geographical cluster methods presuppose underlying spatial similarity in a common area that influences cyclone development (Dacre & Pinto, 2020). Different spatial clustering methods have been used to classify ECC tracks based on synoptic features (Quinting, Catto, & Reeder, 2019), forecast validation (Zheng et al., 2017), genesis location (Browning & Goodwin, 2013, 2016; Kiem et al., 2016), and to determine the impacts or the affected area (Mailier et al., 2006; Pinto et al., 2013). Examples of the different types of clustering methods are reviewed in Section 1.1.

## 1.1 | Cyclone clustering methods

Track clustering studies that use the Poisson and dispersion method primarily focus on seriality and the spatial extent of cyclone counts for an appointed area—with a specific time range or periodically (monthly/annually). This clustering method is useful for determining the areas more affected by cyclone occurrence. By combining polygons with a dispersion statistic (variance to mean ratio) to measure the statistical significance of clusters, potentially affected regions within the study area become apparent. A modification of this method has previously been used in Australian ECL studies, whereby one geographical polygon (herein referred to as the ‘ECL box’; 25° to 40°S and eastern coastline to 160°E) has been used to pre-classify tracks as ECLs before analysis (Cavicchia et al., 2019; Dowdy, Mills, Timbal, & Wang, 2013; Gray et al., 2021; Pepler et al., 2016; Speer et al., 2009, 2021). An alternative approach that did not rely on a defined geographical polygon was adopted by Wolff et al. (2016). That study used a network of hexagonal disks 300 km in diameter spaced 1° apart over the Great Barrier Reef, Australia. Cyclone counts per cell were then converted into a dispersion statistic (similar to Mailier et al., 2006

and Pinto et al., 2013) to determine an over- or underestimate of the distribution of cyclone events against a Poisson model (Wolff et al., 2016).

Fuzzy clustering is another method used to spatially or temporally group cyclone tracks. Data points are assigned to all clusters. The strength of the observation ranges between 0 and 1—equalling one when summed across all clusters. Coefficients equal to one have a higher probability of being included in the corresponding cluster (Kim et al., 2011). Furthermore, unlike *k*-means clustering and other complex mathematical methods, this process offers infinite combinations for track allocation and is thus practical for validating, developing and forecasting scenarios (Zheng et al., 2017).

Another popular clustering method used in cyclone studies is *k*-means clustering (Catto, 2018; Corporal-Lodangco et al., 2014; Kirkland & Zick, 2019; Nakamura et al., 2009; Rahman et al., 2018; Yu et al., 2017). Similar to the Poisson method, *k*-means clustering applies a centroid as a pre-filtering aid in the grouping procedure before the clustering process. In addition, like many statistical processes, *k*-means clustering has an equation adaptable to study specific requirements and can help remove bias (Catto, 2018). This ensures that clusters focus more on the target characteristic (e.g. track shape, length, orientation, size and location; Kirkland & Zick, 2019; Nakamura et al., 2009; Rahman et al., 2018; Yu et al., 2017) to understand cyclone properties (i.e. genesis, intensity and impacts such as regional rainband differences). Cyclones are grouped based on the distance between observations within a population. An Australian study by Quinting, Catto, and Reeder (2019) used this clustering method to identify the synoptic conditions that influence the movement of hybrid cyclones. Events in the Quinting, Catto, and Reeder (2019) study were grouped based on the 315 K potential vorticity anomaly—and a range of cluster numbers (2–10) were tested to estimate the optimal quantity. The best choice was determined using a distance dissimilarity index. This method is also applied in TC and ETC studies when using the MATLAB CCToolbox by Gaffney (2004) and Gaffney et al. (2007). To date, this method has not been applied to ECCs in the Australian region.

The MATLAB CCToolbox developed by Gaffney (2004) and Gaffney et al. (2007) uses probabilistic, curve-aligned clustering and prediction with a regression mixture model—and has been employed in several TC (Camargo et al., 2008; Kossin et al., 2010; Ramsay et al., 2012; Sharma et al., 2021) and ETC studies (Gaffney et al., 2007) in both the Northern and Southern Hemisphere. This toolbox allocates tracks to a specified number of clusters based on their geographical (latitude and longitude) relationship with time. This method

incorporates many aspects of other statistical techniques used for cyclone studies. To determine the ‘optimal’ number of clusters ( $k$ ), a cross-comparison of the maximum log-likelihood (the logarithmic probability of the observed data under the goodness-of-fit metric within the model) and the sum of squared errors (SSEs) of each cluster is conducted (Camargo et al., 2008; Gaffney, 2004; Gaffney et al., 2007; Kossin et al., 2010; Sharma et al., 2021). The present study used the toolbox developed by Gaffney (2004) and Gaffney et al. (2007) because of the flexibility and robustness of the statistical processes available to study cyclone tracks. In addition to applying the toolbox, our clustering methodology employs a pre-filtering process of the tracks to remove bias (seen in Kim et al., 2011; Mailier et al., 2006; Mumby et al., 2011; Nath et al., 2015; Pinto et al., 2013; Wolff et al., 2016)—and dual dissimilarity matrices and  $k$ -means to determine the ‘optimal’ number of clusters. Allocated tracks can then be explored based on a variety of characteristics.

## 1.2 | Aims and significance

ECCs have a significant impact on eastern Australia and previous studies of ECC characteristics and their drivers have either: (a) primarily focused on the location of cyclone development (rather than the cyclone track); (b) covered a restricted geographical range (i.e. have not captured all ECCs outside the ECL box); or (c) used small datasets or a case study approach (limited temporal range). Consequently, our understanding of these systems is incomplete. The review above highlighted that track clustering methods, traditionally applied to TCs (Camargo et al., 2008; Kossin et al., 2010; Ramsay et al., 2012; Sharma et al., 2021) and ETCs (Gaffney et al., 2007), may bridge the gap in exploring characteristics of ECCs such as typical propagation pathways, speed, duration, maximum intensity and ECC impacts. Therefore, the objectives of this study are to:

1. Identify key pathways (clusters) of Australian ECC events from 1950 to 2019 through the application of the MATLAB CCToolbox developed by Gaffney (2004) and Gaffney et al. (2007);
2. Classify and investigate any long-term trends in the frequency of track characteristics, seasonality and intensity per cluster;
3. Analyse the spatial extent of event rainfall for each cluster; and
4. Determine any broadscale environmental conditions (e.g. SST patterns) that could be conducive to cyclone and rainfall genesis.

## 2 | DATA

### 2.1 | Cyclone database

Cyclone data from 1950 to 2019 were sourced from the NCEP1 (National Centres for Environmental Prediction) low-pressure subset (Pepler, 2020a, 2020b). The database was generated using the tracking algorithm/method in Pepler et al. (2015) and the University of Melbourne cyclone tracking scheme (Murray & Simmonds, 1991; Simmonds et al., 1999). The database has several advantages over other Australian cyclone databases (Gray et al., 2021). The database uses the NCEP/NCAR reanalysis database that is re-gridded on a polar projection and extends from 10° to 80°S and 80° to 190°E (Kalnay et al., 1996; Pepler, 2020b). Tracks are generated in 6-h intervals with a 2.5° resolution.

### 2.2 | Rainfall data

Rainfall data from the Queensland (QLD) Government Long-Paddock Scientific Information for Land Owners (SILO) database (Jeffrey et al., 2001) were used in this study. The SILO daily rainfall database spans from 1889 to present and is composed of both point and gridded data variations (derived from both splining and kriging). Our study specifically employed the gridded version of SILO, which uses a 0.05° grid and point data sourced from the Australian Bureau of Meteorology (Jeffrey et al., 2001). SILO covers the region from 10° to 44°S and 112° to 154°E.

### 2.3 | Climate indices

For this study, the Niño 3.4 index (representing ENSO, 5°S–5°N, 170°–120°W; Risbey et al., 2009), the Dipole Mode Index (DMI, representing the IOD) and SST were sourced from the Extended Reconstructed Sea Surface Temperature version 5 (ERSSTv5; Huang et al., 2017). The DMI represents the difference in SSTs between the tropical west (10°S–10°N, 50°–70°E) and the southeastern Indian Ocean (10°S–equator, 90°–110°E; Risbey et al., 2009). ERSSTv5 has a spatial resolution of 2° × 2° horizontal grid, with global coverage, and spans from January 1854 to the present (Huang et al., 2017) at a monthly scale. The database was generated from the International Comprehensive Ocean–Atmosphere Data Set (ICOADS; Risbey et al., 2009). The monthly SAM index was sourced from the Royal Netherlands Meteorological Institute (KNMI) climate explorer (KNMI Climate Explorer, 2022). The SAM index uses the difference of



NCEP/NCAR Reanalysis 1 sea level pressure at level 40 and sea level pressure at level 65. This particular SAM index was chosen because it spans from 1948 to current, thus including the whole study period.

### 3 | METHOD

#### 3.1 | Tracks and database development

It is common practice to pre-classify cyclone tracks (based on length, duration and intensity) before the clustering method is applied (Kim et al., 2011; Mailier et al., 2006; Mumby et al., 2011; Nath et al., 2015; Pinto et al., 2013; Wolff et al., 2016). Therefore, the methods and ECC definition outlined in Gray et al. (2021) were used to create this study's dataset. Following the same criteria, ECC events were defined using the Laplacian method and the NCEP1 dataset from Pepler (2020a; 2020b). To be included in the dataset, events had to be a closed low with a maximum Laplacian (MLAP) value of 0.25 or greater and have at least one data point within the ECL box (25°–40°S—and eastern coastline to 160°E; Speer et al., 2009; Browning & Goodwin, 2013; Dowdy, Mills, & Timbal, 2013; Pepler, Coutts-Smith, & Timbal, 2014; Pepler et al., 2015; Pepler, 2020b). In addition, included tracks were required to have points with a Laplacian value of 0.25 or greater in the ECL box (Gray et al., 2021).

#### 3.2 | Clustering track analysis

Tracks were clustered using the CCToolbox (sourced from <http://www.datalab.uci.edu/software/CCT/#Down>) for MATLAB and the method outlined in Gaffney (2004) and Gaffney et al. (2007). A quadratic polynomial was used for the trajectory of the regression curves because it provided the best representation of fitted versus actual track data (Camargo et al., 2008; Kossin et al., 2010; Ramsay et al., 2012; Sharma et al., 2021). Twenty regression curves were trialled, each with 100 iterations randomly shuffled per run (Camargo et al., 2008; Kossin et al., 2010; Ramsay et al., 2012; Sharma et al., 2021). The curve area that shows a diminishing improvement indicates the optimal number of clusters (using the SSE and maximum log-likelihood; Figure 1). As the number of clusters increases, the cluster spread decreases, reducing the statistical cluster significance by incorporating fewer events within each cluster and reducing the sample size (Camargo et al., 2008; Kossin et al., 2010). Following the method in Camargo et al. (2008), we cross-validated the ECC tracks using a simple random sampling method without replacement. Fifty percent of the track

population was randomly sampled and re-run 100 times. Coefficients (alpha and beta) were identified and organised into quartiles. The original database (100%) and random subset (50%) were displayed via boxplots (Figure S1). The median of each distribution was compared to ensure that the two populations were similar and that the cluster analysis was valid.

#### 3.3 | Intensification and track characteristics

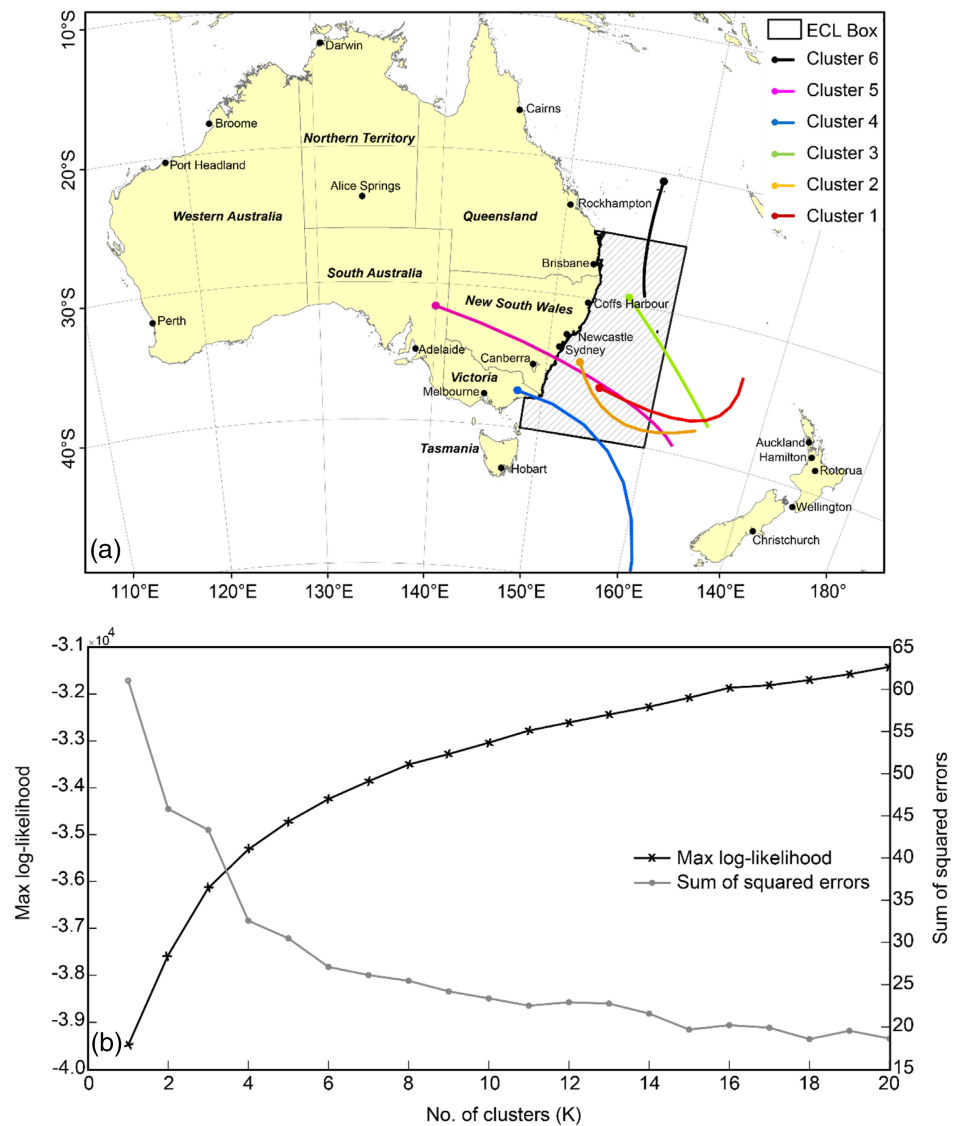
We analysed all events within the compiled database (see Section 3.1), with the timing of ECC genesis used to assign the month and year to individual tracks. Superposed epoch analysis (SEA) was used to examine the differences in intensification patterns of ECC events between clusters, highlighting the average intensity of events in each cluster  $\pm 2$  days on either side of the MLAP value. The mean (and median) track duration, distance travelled, speed and time near land were calculated and compared for each cluster. Furthermore, a seasonal breakdown (percentage) of the number of storms within each cluster was also included. The time near land of each cluster was calculated by extracting the time-steps of each cyclone that occurred on land or within 100 km from the coastline and averaging it over the cluster. Each time-step is counted as 6 h.

A Kruskal–Wallis and post-hoc Tukey–Kramer test (Kirkland & Zick, 2019) were applied to investigate the difference in mean track length, duration and speed in the different clusters. Annual temporal trends for cyclone occurrence were tested using a non-parametric Mann–Kendall test with the TREND eWater Toolkit (Chiew & Siriwardena, 2005). Trends in a Mann–Kendall test are established by examining the S- and Z-values. A high positive (low negative) S-value suggests an upward (downward) pattern. Furthermore, a negative (positive) Z-value that exceeds the level of significance tested shows a downward (upward) trend (Warren & Gilbert, 1988). There is no meaningful change if the Z-value does not exceed the significance level. Significant statistical results were further analysed using a Mann–Whitney U test (non-parametric version of an independent two-sample t-test) to determine if there was a difference within the median of annual events during 1950–1978 and 1979–2019 (Weaver et al., 2018).

#### 3.4 | Rainfall impacts

The rainfall tracking toolbox (*rainfall\_tracker*) by Jaffrés and Gray (2023) was employed to identify each cluster's

**FIGURE 1** The six clusters (a) based on the recommended number of clusters from (b) the log-likelihood value, the sum of squared errors and the law of diminishing returns. The east coast low (ECL) box (black-lined box) and mean regression curves ('storm tracks') were plotted for each cluster. The closed circle is the mean origin of storms in each cluster. [Colour figure can be viewed at [wileyonlinelibrary.com](https://onlinelibrary.wiley.com)]



total event rainfall based on the daily SILO precipitation data. *rainfall\_tracker* first centres a 500 km radius (this can be changed based on users' definition) around each track point and 'clips' the rainfall slice from the SILO dataset corresponding to that cyclone's specific timestep. Although conservative, upon considering other extratropical and rainfall studies (e.g. Cavicchia et al., 2018; Lim & Simmonds, 2007; Pepler, Coutts-Smith, & Timbal, 2014; Pinto et al., 2013; Priestley et al., 2017) that have used a range of radii (50–1000 km), these studies focussed on land-based rainfall with a predominance of tracks having minimal interaction with the coastline. Therefore, a 500 km ( $\sim 5^\circ$ ) radius was selected to identify heavier rainfall closer to the cyclone's centre in comparison to a larger radius (1000 km) that may include additional synoptic features (e.g. troughs and frontal systems) in the output (Pepler et al., 2018; Pepler, Coutts-Smith, & Timbal, 2014; Pinto et al., 2014).

The track and rainfall data had to be temporally aligned to ensure correct overlapping periods are matched since the track is at UTC + 0 and the rainfall is at UTC + 10, but with a 9 a.m. cut-off on the reporting date (Jaffrés & Gray, 2023). For example, the rain assigned to the 8th of June 2007 (rain day) corresponds to rain falling over the period of post-9 a.m. on the 7th of June to 9 a.m. on the 8th of June at UTC + 10. Consequently, the 24-h storm period immediately after 11 p.m. on the 6th of June UTC + 0 aligns with that rain day. In addition, a 1-h time window was used to identify additional rainfall associated with the cyclone event. However, relevant rainfall may be excluded when a track transgresses over different time zones (Jaffrés & Gray, 2023). Collated rainfall slices (per event) were then used to find the 50th (median), 75th and 99th percentiles of event total rainfall per cluster to explore the land-based rainfall impacts.

### 3.5 | Influence of climate drivers

An SST composite for each cluster was generated to identify SST anomalies during the genesis month of that cluster's storm events. This composite was used to reveal the broadscale conditions typically associated with each cluster collectively and seasonally. SST values were detrended per month and grid cell, and the long-term median of the whole database was subtracted from each value to produce the anomalies. The long-term median SST was taken over the entire period (1950 to 2019) instead of the standard 30-year World Meteorological Organization (WMO) period. This was to avoid any bias in recent SST variability by applying a longer and more representative baseline. Statistical significance was tested using a paired Student's *t*-test. Areas of significance were highlighted using the 'stipple' function from the Climate Data Toolbox for MATLAB (Greene et al., 2019).

Anomalies were used to determine local environmental conditions and features influencing the different clusters. The ENSO and SAM phase corresponding to each storm's genesis month was identified based on the sustained monthly Niño 3.4 and SAM ( $\pm 0.5$ ) index (National Center for environmental information [NOAA], 2022). Positive (negative) Niño 3.4 index values correspond to El Niño (La Niña) conditions. A similar process for the IOD was applied using sustained monthly values of  $\pm 0.4$  (Australian Bureau of Meteorology, 2022).

The recurrence interval (or return period) for cyclones per cluster was calculated by using the total number of months of each phase (from 1950 to 2019) divided by the total number of cyclone events that occurred in the corresponding phase. This method was then repeated for each seasonal subset. The statistical significance of the cyclone recurrence interval (in months) in the different climate phases (positive, negative and neutral) was evaluated using a test of proportions (Gray et al., 2020; Hogg & Tanis, 1988; Verdon, Kiem, & Franks, 2004). For this test, the total number of ECCs within each phase (e.g. positive ENSO [ $y_1$ ]) was first divided by the total number of months in that same phase ( $n_1$ ) over the 1950–2019 period (ratio  $P_1$ ). Similarly, for each pair (e.g. positive [ $y_1$  and  $n_1$ ] vs negative ENSO [ $y_2$  and  $n_2$ ]), the combined count was obtained (total number of cyclones in either phase, divided by total number of months in these phases):  $P_{12} = (y_1 + y_2)/(n_1 + n_2)$ . The test statistic was then derived from testing the hypothesis of  $P_1 = P_2$  (Gray et al., 2020; Hogg & Tanis, 1988; Verdon, Kiem, & Franks, 2004). This test was applied for the recurrence intervals over both the total period (from 1950 to 2019) and the seasonal subsets. However, only the overall (annual), JJA (June,

July and August) and SON (September, October and November) results have been discussed further, with autumn and summer results presented in the supplementary section S1.

## 4 | RESULTS

### 4.1 | Clustering analysis and track characteristics

Six clusters were found to be the optimal number for this study based on the SSE and maximum log-likelihood analyses (Figure 1). When comparing the characteristics of the six clusters, three broad groups become apparent based on storm genesis location: coastal (C1 to C3; Figure 2), continental (C4 and C5; Figure 3) and tropical (C6; Figure 4). Clusters 1 to 3 (Figure 2) are relatively close to the eastern seaboard, and the genesis locations are within the ECL box. The main differences between these three clusters are their genesis location and track shape. These three clusters comprise the majority (72%) of the cyclones identified in this study. C1 tracks (Figure 2a) are situated primarily within the ECL box's southeastern corner, mainly traversing away from the coastline and making up 29% (175 events; Table 1) of the total number of cyclones ( $n = 598$ ) in this study. C2 tracks (Figure 2e) embrace the coastline (western side of the ECL box)—centred around Sydney to the central coast—and contribute 15% (90 events; Table 1) of the total number of cyclones. Lastly, C3 tracks (Figure 2i) are positioned along the coastline but in the northern half of the ECL box towards the QLD and NSW border and provide 27% (163; Table 1) of storms from 1950 to 2019.

All three coastal clusters (C1, C2 and C3) are more frequent in the austral winter months (JJA; Figure 2c, g, k), with C1 and C3 contributing over 60% of JJA storms from 1950 to 2019 (Table 1). C1 events are prominent throughout the year, with the number of events increasing into late winter and spring (Figure 2c). C3 events are similarly prominent throughout most of the year, except during austral spring (Figure 2k). All three clusters exhibit a relatively steady build-up and decay before and after reaching their MLAP (Figure 2b, f, j). Slightly higher intensities (relative to C3) are observed for C1 and C2 after reaching maximum intensity, with C3 having the lowest intensity overall. In all three clusters, intensities 24 h after MLAP tend to remain higher than the average intensity of the 24-h period before MLAP. For the coastal clusters, C2 has a longer duration ( $\sim 7$  h) near land when compared to C1 ( $\sim 1.5$  h) and C3 ( $\sim 4.5$  h; Table 1). However, C3 yields a significant downward trend ( $p = 0.0045$ ; Table S1) between 1950 and 2019. This trend could be

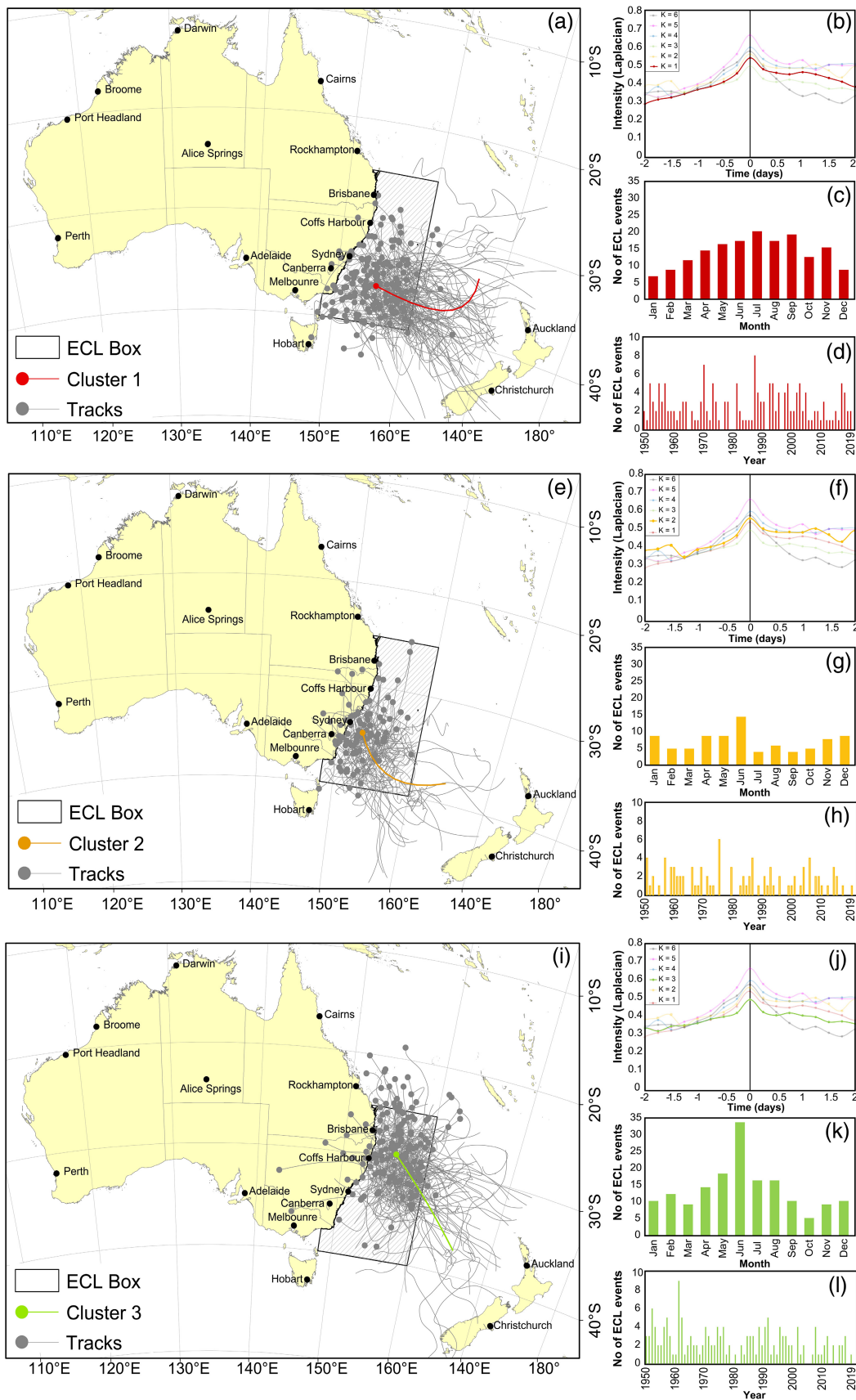


**FIGURE 2** Coastal-focused cyclones are contained within C1, C2 and C3. Track maps highlight the genesis and orientation of tracks (a, e and i). SEA graphs (b, f and j) are used to highlight the cluster means for 2 days before and after reaching maximum intensity (MLAP). Monthly (c, g, k) and annual (d, h and l) patterns are used to determine seasonal or long-term trends. [Colour figure can be viewed at [wileyonlinelibrary.com](http://wileyonlinelibrary.com)]



attributed to more events being present during individual years before 1980 (especially 1961, with nine events counted for that year alone; Figure 2I). Further statistical analysis (Mann–Whitney  $U$  test; Table S2) identified that

the median number of annual C3 storm events during the 1950–1978 period is significantly larger ( $p = 0.008$ ) than that of the satellite period (1979–2019), thus reinforcing the downward trend.

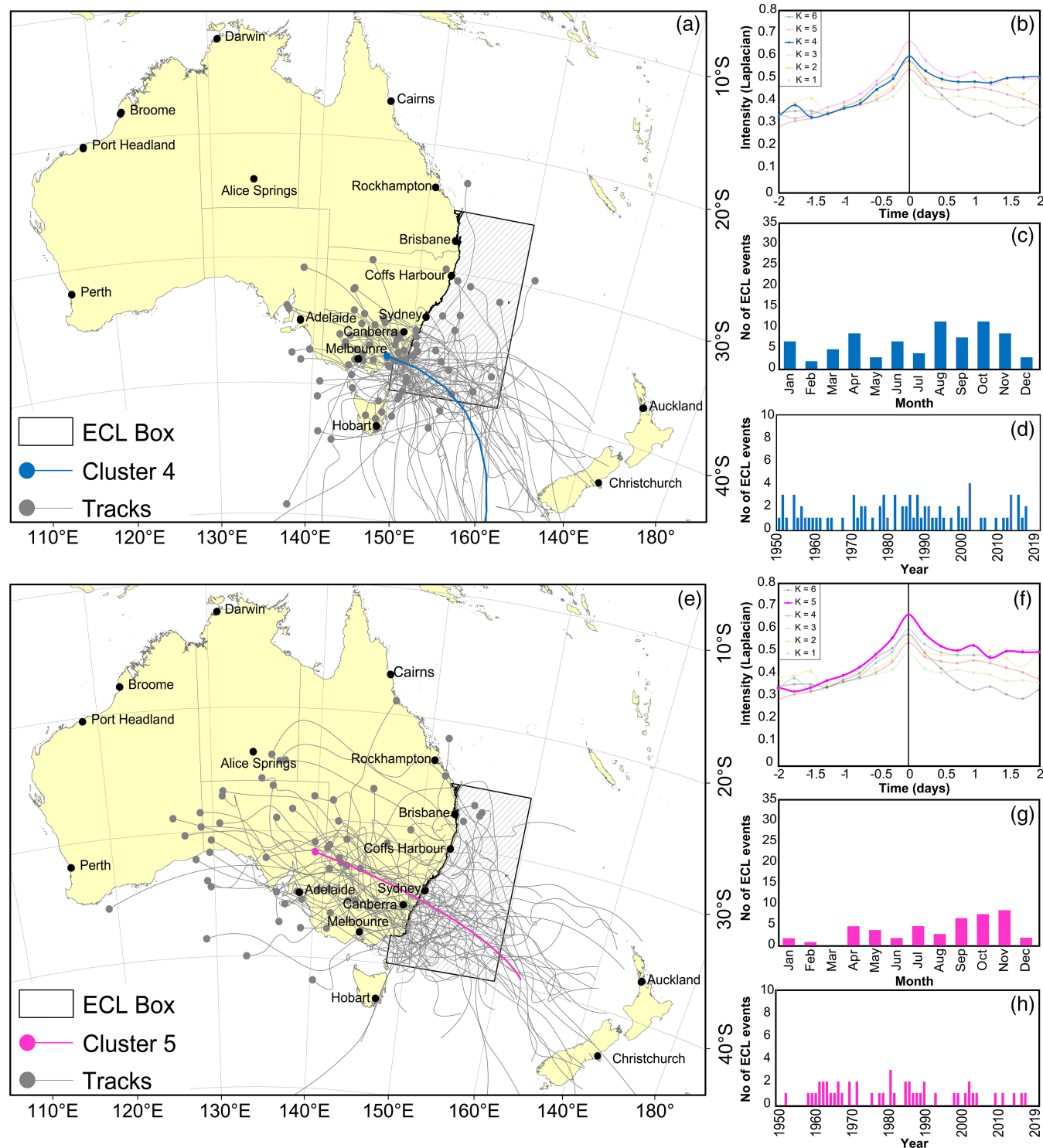


**FIGURE 3** Continental cyclones are contained within C4 and C5. Track maps highlight the genesis and orientation of tracks (a and e). SEA graphs (b and f) are used to highlight the cluster means for 2 days before and after reaching maximum intensity (MLAP). Monthly (c and g) and annual (d and h) patterns are used to determine seasonal or long-term trends. [Colour figure can be viewed at [wileyonlinelibrary.com](http://wileyonlinelibrary.com)]

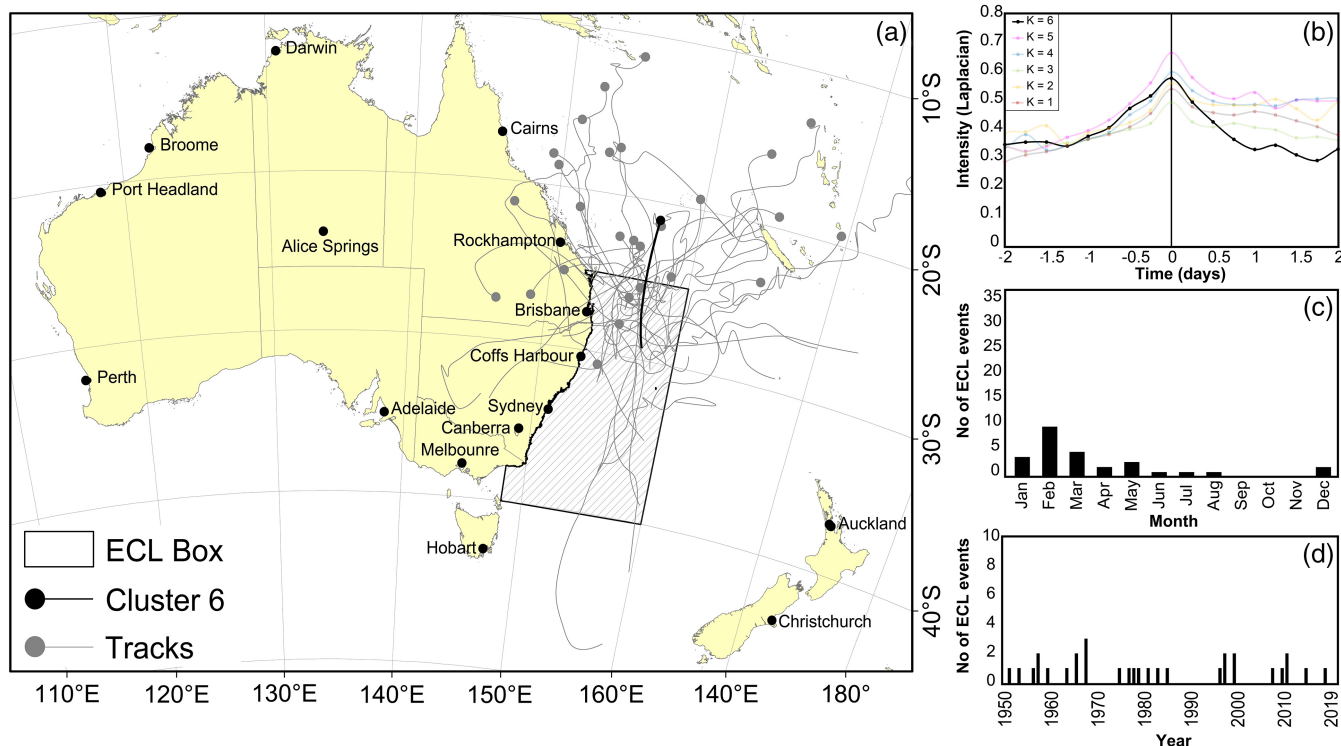


**FIGURE 4** Tropical-influenced cyclones are highlighted within C6. A track map highlights the genesis and orientation of the tracks (a). A SEA graph (b) highlights the cluster means for 2 days before and after reaching maximum intensity (MLAP). Monthly (c) and annual (d) patterns are used to determine seasonal or long-term trends. [Colour figure can be viewed at [wileyonlinelibrary.com](http://wileyonlinelibrary.com)]

**TABLE 1** Seasonal and total count (percentage) of east coast cyclone (ECC) events relative to each cluster, along with total storm numbers and the mean (median) amount of time (hours) near land per cluster.

Cluster	DJF count (%)	MAM count (%)	JJA count (%)	SON count (%)	Total number of storms (%)	Mean (median) time near land (h)
1	25 (22)	44 (30)	57 (31)	49 (33)	175 (29)	1.51 (0)
2	23 (20)	23 (16)	25 (13)	19 (13)	90 (15)	6.88 (6)
3	32 (28)	41 (28)	66 (35)	24 (16)	163 (27)	4.38 (0)
4	12 (10)	18 (12)	23 (12)	29 (19)	82 (14)	15.95 (15)
5	7 (6)	10 (7)	13 (7)	29 (19)	59 (10)	41.80 (36)
6	16 (14)	10 (7)	3 (2)	0 (0)	29 (5)	18.62 (12)

Abbreviations: DJF, December, January, February; JJA, June, July and August; MAM, March, April, May; SON, September, October, November.

Cyclones with an overland genesis (i.e. continental) were grouped into clusters 4 (82) and 5 (59; Figure 3). Continental cyclones compose 24% of the total number of storms from 1950 to 2019 (Table 1). Uniquely, C4 cyclones (Figure 3a) are situated around the Bass Strait. A majority of C4 events develop within or near Victoria or Tasmania. These storm tracks are generally curved, with a southern decay. C5 cyclones (Figure 3e) are more westerly and inland-focused, and the tracks have travelled across or down the continent towards the east coast. No significant long-term trends or seasonality were identified for C4 and C5 (Table S1). C4 and C5 occur more

frequently in austral spring (SON; Figure 3c, g) and collectively contribute 38% of the total number of storms over this period (Table 1). Compared to C5 cyclones, C4 storms are more prevalent during late winter and early spring (Figure 3c, g). The intensification of cyclones in both these clusters is quite rapid (the Laplacian upward of 0.1 within 6 h), with the highest intensity (0.66; Figure 3f) for all six clusters observed for C5. C5 cyclones have the longest track length and average time over/near land (~42 h; Table 1). The mean (36 km h<sup>-1</sup>) and median (34 km h<sup>-1</sup>; Table 2) speed values of C5 are the highest among the six clusters, indicating that they are the fastest

**TABLE 2** Summary of key cluster characteristics from Section. This table contains information on the seasonality and the average (mean and median) track length, intensity, duration and speed. The maximum amount of rainfall and impact location for all the event rainfall (percentiles) are also listed. The last three columns are the dominant phases for ENSO, IOD and SAM based on the recurrence intervals — specific for each season per cluster (discussed further in sections 3.5 and 4.4).

Cluster	Sub-class	Seasonality	Intensity		Median (mean) duration (days)	Median (mean) speed (km h <sup>-1</sup> )	Event rainfall (percentiles)	Observed		
			(mean) cluster MLAP	(mean) length (km)				ENSO conditions	IOD conditions	SAM conditions
1	Coastal	Throughout the year. More events in austral winter: May to September.	0.540	1238 (1331)	1.50 (1.99)	29 (32)	<p><b>50th: No rainfall</b></p> <p><b>75th: Maximum rain: 9.7 mm</b></p> <p>Coffs Harbour to the Victorian/NSW border.</p> <p><b>99th: Maximum rain: 251.9 mm</b></p> <p>Eastern seaboard, including Tasmania. Higher amounts in southern NSW and northern Victoria.</p>	<p><b>DJF:</b> Neutral</p> <p><b>MAM:</b> Neutral</p> <p><b>JJA:</b> Neutral</p> <p><b>SON:</b> Neutral</p> <p>Neutral</p>	<p><b>DJF:</b> Neutral</p> <p><b>MAM:</b> Neutral</p> <p><b>JJA:</b> Neutral</p> <p><b>SON:</b> Neutral</p>	<p><b>DJF:</b> Positive</p> <p><b>MAM:</b> Positive</p> <p><b>JJA:</b> Negative</p> <p><b>SON:</b> Positive</p>
2		Throughout the year. More events in austral winter: April to June.	0.560	989 (1220)	1.75 (2.33)	23 (25)	<p><b>50th: Maximum rain: 35.8 mm</b></p> <p>The central coast of NSW and the eastern corner of Victoria.</p> <p><b>75th: Maximum rain: 69.7 mm</b></p> <p>The Victorian/NSW border to the NSW/QLD border.</p> <p><b>99th: Maximum rain: 362.9 mm</b></p> <p>Inland eastern seaboard, including Tasmania. Higher amounts in southern NSW and northern Victoria, between Melbourne and Coffs Harbour.</p>	<p><b>DJF:</b> La Niña</p> <p><b>MAM:</b> Neutral</p> <p><b>JJA:</b> Neutral</p> <p><b>SON:</b> Neutral</p>	<p><b>DJF:</b> Neutral</p> <p><b>MAM:</b> Neutral</p> <p><b>JJA:</b> Neutral</p> <p><b>SON:</b> Neutral</p>	<p><b>DJF:</b> Positive</p> <p><b>MAM:</b> Positive</p> <p><b>JJA:</b> Positive</p> <p><b>SON:</b> Negative</p>
3		Throughout the year. More events in austral winter: May to August.	0.495	1027 (1279)	1.75 (2.31)	23 (25)	<p><b>50th: Maximum rain: 11.8 mm</b></p> <p>Northern NSW coastline to Brisbane.</p> <p><b>75th: Maximum rain: 49.0 mm</b></p> <p>Northern coast between Sydney and Brisbane.</p> <p><b>99th: Maximum rain: 458.4 mm</b></p> <p>Coastal NSW into inland QLD and southern Victoria. Higher amounts in central to northern</p>	<p><b>DJF:</b> La Niña</p> <p><b>MAM:</b> Neutral</p> <p><b>JJA:</b> Neutral</p> <p><b>SON:</b> Neutral</p> <p>La Niña</p>	<p><b>DJF:</b> Neutral</p> <p><b>MAM:</b> Neutral</p> <p><b>JJA:</b> Neutral</p> <p><b>SON:</b> Neutral</p>	<p><b>DJF:</b> Negative</p> <p><b>MAM:</b> Positive</p> <p><b>JJA:</b> Negative</p> <p><b>SON:</b> Positive</p>

TABLE 2 (Continued)

Cluster	Sub-class	Seasonality	Intensity (mean cluster MLAP)	Median length (km)	Median (mean) duration (days)	Median (mean) speed (km h <sup>-1</sup> )	Event rainfall (percentiles)	Observed ENSO conditions	Observed IOD conditions	Observed SAM conditions
4	Continental	Throughout the year. More events in austral spring: April, August, October and November	0.599	1734 (1803)	2.00 (2.19)	32 (35)	NSW between Sydney and Brisbane.	<b>DJF:</b> El Niño	<b>DJF:</b> Neutral	<b>DJF:</b> Positive
							<b>50th: Maximum rain: 29.1 mm</b> Southern to inland NSW, Victoria and most of Tasmania.	<b>MAM:</b> Neutral	<b>MAM:</b> Neutral	<b>MAM:</b> Positive
5		Common in austral spring. More events occur from September to November.	0.664	2974 (3249)	4 (4.05)	34 (36)	<b>75th: Maximum rain: 50.0 mm</b> Southern and inland NSW, Victoria and most of Tasmania. Extensive rainfall throughout Victoria and west of ACT.	<b>JJA:</b> Neutral	<b>JJA:</b> Neutral	<b>JJA:</b> Positive
							<b>99th: Maximum rain: 294.1 mm</b> East coast to inland NSW, SA and Victoria. Higher rainfall from Coffs Harbour to Melbourne, inner regions of Victoria and the northeastern corner of Tasmania.	<b>SON:</b> El Niño	<b>SON:</b> Neutral	<b>SON:</b> Positive
6	Tropical	More events occur in austral summer, from December to May.	0.579	2180 (2364)	3.75 (4.31)	23 (25)	NSW, QLD, VIC, SA, TAS, ACT and NT. Higher rainfall in central QLD, the south coast of NSW, eastern Victoria and the eastern coastline of Tasmania.	<b>DJF:</b> La Niña	<b>DJF:</b> Neutral	<b>DJF:</b> Negative
							<b>50th: Maximum rain: 132.5 mm</b> NSW to Bundaberg, QLD. Higher rainfall in the top, northeast corner of NSW and southeast QLD.	<b>MAM:</b> Neutral	<b>MAM:</b> Neutral	<b>MAM:</b> Positive
								<b>JJA:</b> Neutral	<b>JJA:</b> Neutral	<b>JJA:</b> Negative
								<b>SON:</b> El Niño		

(Continues)



TABLE 2 (Continued)

Cluster	Sub-class	Seasonality	Intensity (mean cluster MLAP)	Median (mean) length (km)	Median (mean) duration (days)	Median (mean) speed (km h <sup>-1</sup> )	Event rainfall (percentiles)	Observed ENSO conditions	Observed IOD conditions	Observed SAM conditions
							<b>75th. Maximum rain: 359.9 mm</b> Sydney to the north of Rockhampton, QLD. Higher rainfall amounts between Brisbane and Coffs Harbour.			
							<b>99th. Maximum rain: 1144.3 mm</b> Throughout NSW, Victoria and coastal QLD. Higher rainfall in central QLD, central to northern NSW, and the Brisbane area.			

Abbreviations: ACT, Australian Capital Territory; DJF, December, January, February; ENSO, El Niño Southern Oscillation; IOD, Indian Ocean Dipole; JJA, June, July and August; MAM, March, April, May; MLAP, maximum Laplacian; NSW, New South Wales; NT, Northern Territory; QLD, Queensland; SA, South Australia; SAM, Southern Annular Mode; SON, September, October, November, TAS, Tasmania; VIC, Victoria.

cyclones within this region. C5 is closely followed by C4, with mean (median) speeds of 35 km h<sup>-1</sup> (32 km h<sup>-1</sup>) for the latter (Table 2).

Storm events that begin in, near or are influenced by the tropics are grouped in C6 (Figure 4). C6 contains 5% ( $n = 29$ ) of the total number of cyclones ( $n = 598$ ) from 1950 to 2019. Most events originate in the northern portion or outside the ECL box. These events can be classified as tropical lows or TC remnants (Browning & Goodwin, 2013; Kiem et al., 2016; Speer et al., 2009), supported by the prevalence of these events during the austral summer months (Table 1; Figure 4c). However, these storms only make up 14% of the seasonal total for summer events from 1950 to 2019 (Table 1). In addition, this type of storm is not active or present in spring. C6 cyclones display a slow but intense build-up — and sudden decay after reaching maximum intensity (Figure 4b). As with most other clusters (C1, C2, C4 and C5), no statistically significant long-term trend in C6 occurrence was detectable since 1950 (Table S1; Table S2). Conversely, C6 has the highest mean track duration (4.3 days; Table 2) and the second-longest amount of time over/near land (~19 h; Table 1).

The mean and median track lengths, duration, speed and time near land (h) were identified between clusters (Table 2). The cyclone attributes (i.e. speed, duration, length, time near land) in C2 and C3 are very similar. The  $p$ -value (<0.001; Table S3) of the Kruskal–Wallis test demonstrated a significant difference between the mean duration, speed and length between the six clusters. After the Kruskal–Wallis test (Table S3), the mean speed, length and duration differences between each pairwise combination of groups were compared with a post-hoc Tukey–Kramer test (Table S4).

Differences in duration are present in C1 to C4 versus C5 and C6 (Table S4). The track distance combinations that did not differ were C1 versus C2 and C3; C2 versus C3; and C4 versus C6. All other combinations had a significant mean difference. Cluster combinations with significant differences in speed include C1 against C2 and C3; C2 versus C4 and C5; C3 versus C4 and C5; and C6 against C4 and C5 (Table S4).

## 4.2 | Rainfall impacts for the six ECC clusters

The rainfall analysis shows that, except for C1, each cluster makes a significant and quantifiable contribution to the precipitation over the east coast of Australia at the 50th percentile (i.e. cluster median event rainfall for each grid point; Figure 5). C2 storms (Figure 5b) contribute widespread rainfall (median between 0 and 50 mm) to

the central coast of NSW and the eastern corner of Victoria. Higher rainfall values are focused on southern NSW and northeastern Victoria. Median rainfall for the tracks in C3 is most significant along the northern NSW coastline to Brisbane (Figure 5c). C4 rainfall is associated with southern NSW (with some stretching to inland NSW), Victoria and most of Tasmania (Figure 5d). Higher rainfall amounts are delivered to Victoria and west of Canberra. Rainfall linked to C5 is spatially more expansive, encompassing most of inland NSW and Victoria into South Australia (Figure 5e). In particular, the NSW south coast and eastern corner of Victoria experience more rainfall from C5 events. C6 median rainfall is the highest for all six clusters and extends from NSW to Rockhampton, QLD (Figure 5f). The prominent focus of median rainfall for C6 is located in the top, northeast corner of NSW and southeast QLD, with values exceeding 100 mm (Table S5).

The 75th percentiles of C2 and C3 rainfall distributions are focused on the coast (Figure 6), similar to the median rainfall. C1 rainfall (0–5 mm) is minimal at the 75th level (Figure 6a). C2 third quartile rainfall is more widespread, with greater quantities (70 mm; Table S5) around the Victorian/NSW border (Figure 6b). The 75th percentile rainfall for C3 (Figure 6c) occurs more northerly than for C1 and C2, falling in the region between Sydney and Brisbane (Figure 6). Conversely, C4 (Figure 6d) and C5 (Figure 6e) 75th percentile rainfall exhibits a more inland distribution. C4 impacts on rainfall are located more southerly (towards Victoria and Tasmania), whereas the C5 rainfall focus is more to the west (reaching into South Australia). In addition, only these two clusters bring rainfall to Tasmania based on the 75th percentile. C6 third quartile rainfall has a more extensive coastal coverage (Figure 6e). Third-quartile rainfall values mainly range from 1 to 100 mm, although up to 359.9 mm have been obtained (Table S5).

Rainfall is more widespread for all clusters at the 99th percentile (Figure 7). The 99th percentile rainfall associated with C1 reaches 252 mm (Table S5), and the impacts span across the eastern seaboard, including Tasmania (Figure 7a). The highest rainfall values for C1 occur in southern NSW and northern Victoria. For C2, the rainfall zone covers the same areas as C1 but advances further inland (Figure 7b). Higher rainfall areas are present along southern NSW and Victoria, reaching 362.9 mm (Table S5). The rainfall in C3 is mainly focused along coastal NSW (Figure 7c), although lower amounts (<200 mm) extend inland up to QLD and south to Victoria. Rainfall depths greater than 450 mm (the highest total equating to 458 mm; Table S5) are present along the central to northern NSW coast for C3 events. The

potential impact zone for C4 is also widespread, with extreme rainfall amounts of 294 mm (Figure 7d; Table S5). However, the areas with higher rainfall are the north and south coast, inner areas of Victoria and the northeastern corner of Tasmania. Rainfall from C5 cyclones has the greatest spatial coverage, extending over all six states and two territories (Figure 7e). Areas of higher rainfall (>200 mm) are present in central QLD, the south coast of NSW, eastern Victoria and the eastern coastline of Tasmania. The highest event rainfall is associated with C6 (Figure 7f). Precipitation (>350 mm) is focused along the coast in central QLD, central to northern NSW and the Brisbane area. Rainfall up to 150 mm can occur within C6 ECC events throughout NSW, Victoria and coastal QLD. The maximum rainfall depth for C6 is 1144 mm (Table S5).

### 4.3 | SST anomalies for each ECC cluster

SST anomalies were generated for the most common seasons in terms of cyclone occurrence, i.e. austral winter (JJA) and spring (SON). A combined version of SST composites (covering the entire year) is presented in Figure S2.

The winter SST anomalies in C1 suggest a weak central Pacific El Niño as the warm tongue extends along the equator (Figure 8a; Freund et al., 2021). Other notable warmer-than-average SSTs are evident in the southern Indian Ocean. The composite SST pattern associated with C2 (Figure 8b) also highlights significantly warmer SSTs in the Indian Ocean, extending southwards along the northwestern coast of Australia near Indonesia. There is a small area of cooler water in the western Pacific near Chile, but the location and shape are not prominent enough to link directly to ENSO. Overall, the SSTs for C3 are warmer than average (Figure 8c) and significant anomalies are present in the northwestern Pacific near Asia and the Indian Ocean. In addition, significant temperature anomalies (outlined via stippling) for C3 cyclones are present in the southwestern Pacific Ocean and the Australian east coast.

The winter SST pattern for C4 suggests a weak El Niño—a warm tongue along the equatorial central Pacific and two cooler water bodies on either side (Figure 8d; Freund et al., 2021)—with areas of significance located within this formation. Waters around Australia are not significant, with warmer than usual SSTs located to the south of Tasmania and the north of the Northern Territory. At the same time, cooler waters occur within waters of the northeastern and west coasts. SST anomalies are more La Niña like for C5 ECCs, resulting from warmer-than-average conditions around

Australia's northern and eastern coastline. Widespread, significant SST anomalies are also present for C5 in the Southern Ocean, Indian Ocean and New Zealand region. These conditions also suggest an IOD-positive pattern (warmer temperatures in the western Indian Ocean) for C5 SST conditions (Figure 8e). C6 SST anomalies have the most extreme signature (in terms of the strength and significance of the associated SST anomalies; Figure S3). This is because there are only three cyclone events present for C6 during JJA, generating a more extreme result. Cool pools are located near eastern Australia, the eastern and central equatorial Pacific Ocean—suggestive of a La Niña signal—with areas of significance highlighted by stippling along the equatorial central pool.

The SST anomalies associated with austral spring (SON) cyclones for each cluster are shown in Figure 9. C1 SSTs around Australia exhibit a cooler-than-average SST pool in the north/northeast and two warmer pools—one along the east coast and the other along the northwestern coast. Significant SST anomalies exist in the eastern and northern Pacific and the Southern Ocean near Africa. C2 SST anomalies indicate warmer than average conditions, with areas of significantly higher temperatures in both the northern and southern Pacific Ocean (Figure 9b). Cooler SSTs are present along the central Pacific, which could suggest a weak La Niña; however, their connection to Western Pacific SSTs is inconclusive. The SSTs around northern and eastern Australia are anomalously warm although significance around the continent is limited. Warmer than average SST anomalies are widespread for C3 (Figure 9c), with the essence of an El Niño beginning to form within a significant warm pool in the eastern Pacific. Another significantly warmer region is located in the Indian Ocean near southern Africa. Furthermore, the SSTs around the northern part of Australia are warmer.

Consistent with their winter SST relationships signature, the SST anomaly pattern for C4 is suggestive of central Pacific El Niño events, further reinforced by a significant relationship to SSTs in the central body of the warm tongue (Figure 9d). There is also an area of significantly warmer water in the southern Indian Ocean. Notable SST anomalies around Australia are present along the northwestern coastline with a warmer pool and a cooler area around the tip of QLD. SST anomalies in spring for C5 ECCs show that SSTs tend to be significantly warmer than average (Figure 9e) around the majority of western and southern Australia, specifically in the Tasman Sea and the Southern Ocean below Western Australia. Additionally, cooler water is found along the eastern coastline of QLD. No results are presented for C6 because of the absence of storms in that cluster in spring.

#### 4.4 | The influence of large-scale climate modes on ECCs

Differences in the probability of cyclone events in the six clusters occurring in a positive phase (El Niño, IOD-positive, SAM-positive)—in comparison to ECCs developing in a negative (La Niña, IOD-negative, SAM-negative) and/or neutral phase—were investigated using tests of proportions. The recurrence intervals of cyclones between 1950 and 2019 in each cluster vary depending on the prevalence of the relevant climate phenomena (Table 3) and their phase (Table 4; Table 5; Table 6). For example, a value of 4.9 for C1 cyclones (Table 4) means that, on average, there is one C1 event every 4.9 months during the positive phase of ENSO (i. e. for every five, not necessarily consecutive months in the positive ENSO phase, approximately one C1 event forms). Lower recurrence intervals equal more frequent storms.

Overall, ECC genesis most often occurs during neutral ENSO conditions. In particular, the number of C3 events is most common in neutral months. C1 to C5 have approximately double the likelihood of occurring in a neutral phase than a La Niña (with the result for C1 and C3 statistically significant at  $\alpha = 0.01$ ; Table 4). Some ECC events that are generated in neutral ENSO months correspond to transitioning periods of the Niño 3.4 index (e.g. C1 events during 2001; Figure S4). Although ECC genesis commonly occurs in neutral ENSO conditions, the combined and seasonal analyses demonstrate that events can be generated under favourable extreme conditions (either El Niño or La Niña; Table 4). However, statistically, significantly different results are predominately between the neutral and an extreme phase. For example, C2 events had a significantly lower likelihood of events forming in El Niño compared to ENSO neutral ( $p = 0.007$ ; Table S6).

The overall frequency of ECCs in the two extreme ENSO phases is comparable (with a similar finding for IOD and SAM). Nevertheless, individual clusters may preferentially occur in one type of extreme phase, although this bias varies on a seasonal scale. Specifically, C1 events are more frequently generated in El Niño conditions (cyclone recurrence interval approximately every 5 months from 1950 to 2019; Table 4) when compared to La Niña periods. Conversely, La Niña months have more C3 ECCs than El Niño months but fewer than neutral months. Differences in C3 cyclone occurrence between neutral phases versus La Niña or El Niño are statistically significant ( $p < 0.001$ ), whereas La Niña versus El Niño events are not ( $p = 0.035$ ; Table 4 and Table S3). Furthermore, the occurrence of cyclones during El Niño conditions appears to have increased after 1979 (also

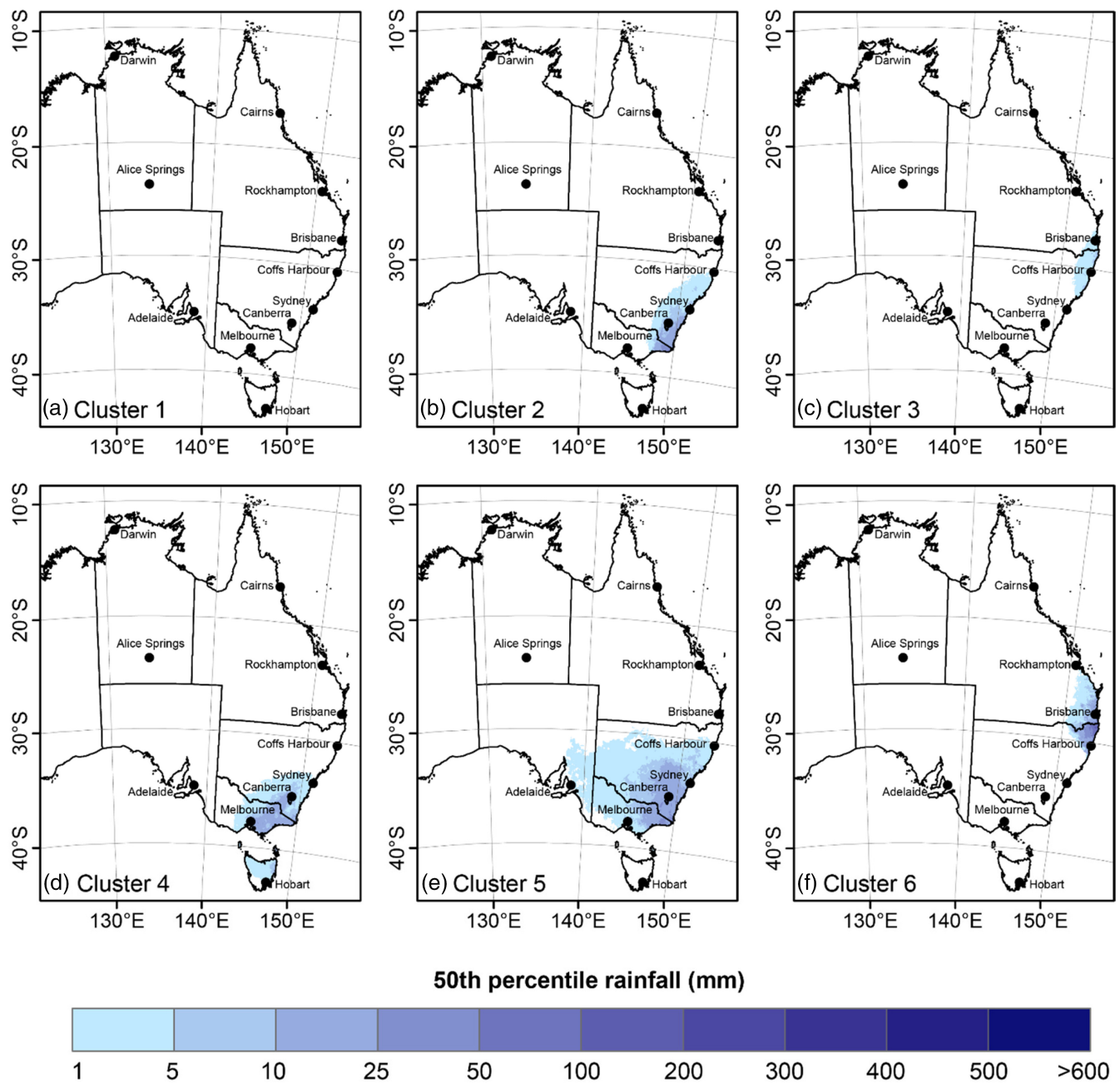


**FIGURE 5** The 50th percentile plots are used to determine the areas impacted by median event rainfall (mm) for each cluster. Areas of lower (higher) precipitation are highlighted in lighter (darker) colours. Plots are set out in consecutive order of cluster number. [Colour figure can be viewed at [wileyonlinelibrary.com](https://onlinelibrary.wiley.com/terms-and-conditions)]

corresponding to an increase in El Niño frequency) for C1 and C3 (Figure S4).

Preferential occurrence on a seasonal scale is emphasised during JJA for C3 combinations that include ENSO-neutral. For example, a significant difference for cyclone return periods was observed when comparing neutral C3 ECCs to La Niña or El Niño events (Table 5; Table S7). C6 cyclones were more (less) common to occur during DJF (JJA), with a significant difference in La Niña versus El Niño phases during austral summer. Combined, only

three C6 events were generated during JJA and SON. Consequently, no significant differences in C6 recurrence intervals were present in ENSO combinations during JJA (Table 5) and SON (Table 6).

Similar to ENSO, many cyclonic events formed during an IOD-neutral phase in the six clusters throughout the year (Table 4; Figure S5). C6 events are most frequent during neutral IOD, attributable to the preferential occurrence of these storms during the DJF months and the absence of IOD during that season, with the reverse



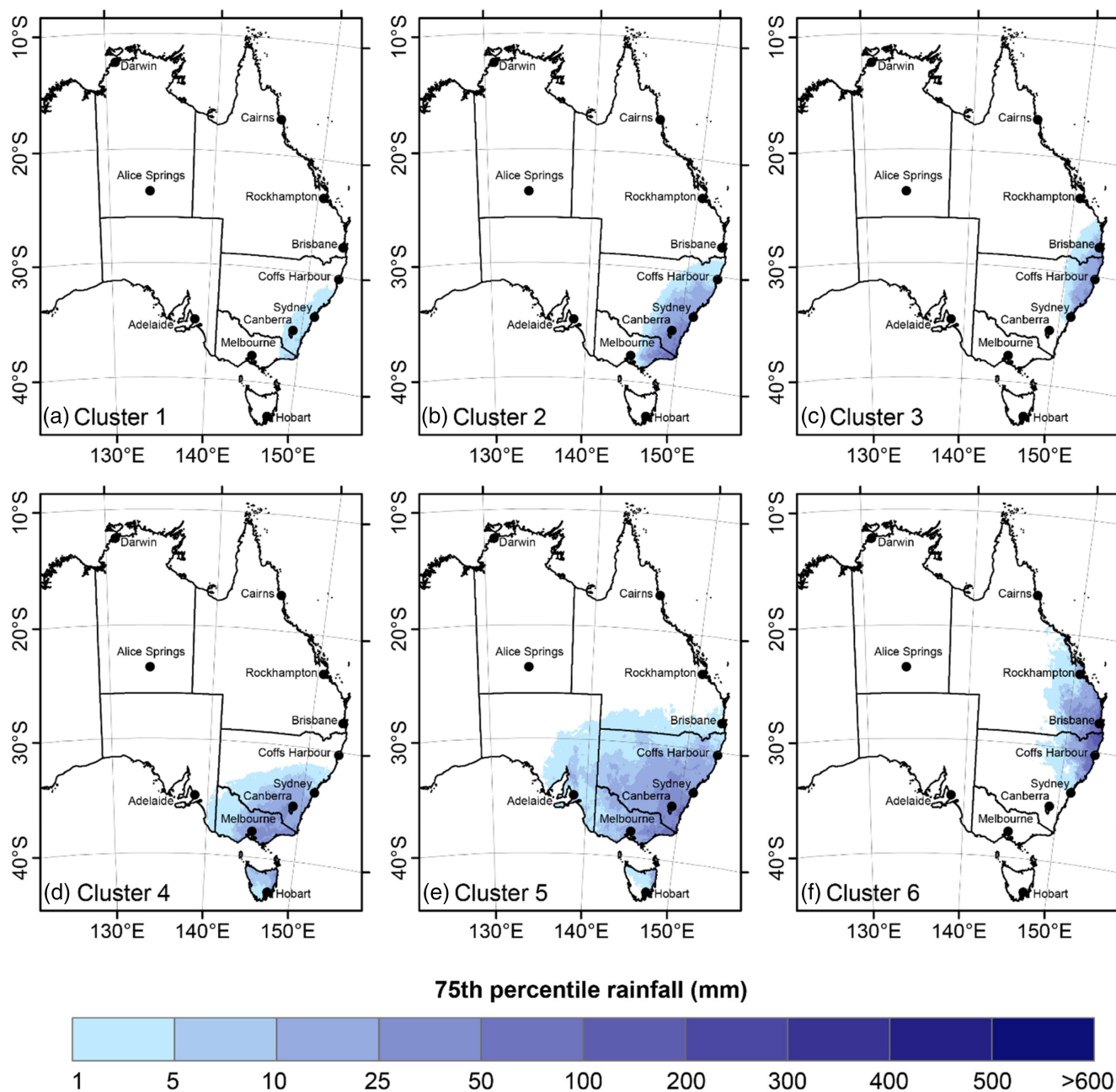


**FIGURE 6** The 75th percentile plots are used to determine areas impacted by rainfall (mm) at the third quartile for each cluster. Areas of lower (higher) precipitation are highlighted in lighter (darker) colours. Plots are set out in consecutive order of cluster number. [Colour figure can be viewed at [wileyonlinelibrary.com](http://wileyonlinelibrary.com)]

(rare C6 storm genesis) during the peak IOD period (June–November; Pepler, Timbal, et al., 2014; Risbey et al., 2009; Verdon-Kidd, 2018). Overall, only two C6 ECCs were generated in non-neutral IOD months, thus producing very long recurrence intervals (Table 4). Neutral IOD phases are also consistently associated with the most frequent storm genesis during JJA (Table 5) and SON (Table 6), with a significant reduction in cyclone numbers for positive and negative IOD phases compared to neutral months.

Particularly large decreases in C2 cyclone frequency are evident during IOD-positive JJA (and C1 and C2 events during IOD-negative SON), resulting in statistically significant differences between IOD-neutral and extreme phases (Table 4 to Table 6). During IOD-positive phases, C3 contains the highest number of ECC events ( $n = 21$ ) out of all clusters (overall return period every 13.3 IOD-positive month; Table 4), with 1961 exhibiting six events (Figure S5). However, C1 cyclones have comparable values ( $n = 20$  and recurrence interval of 14.0

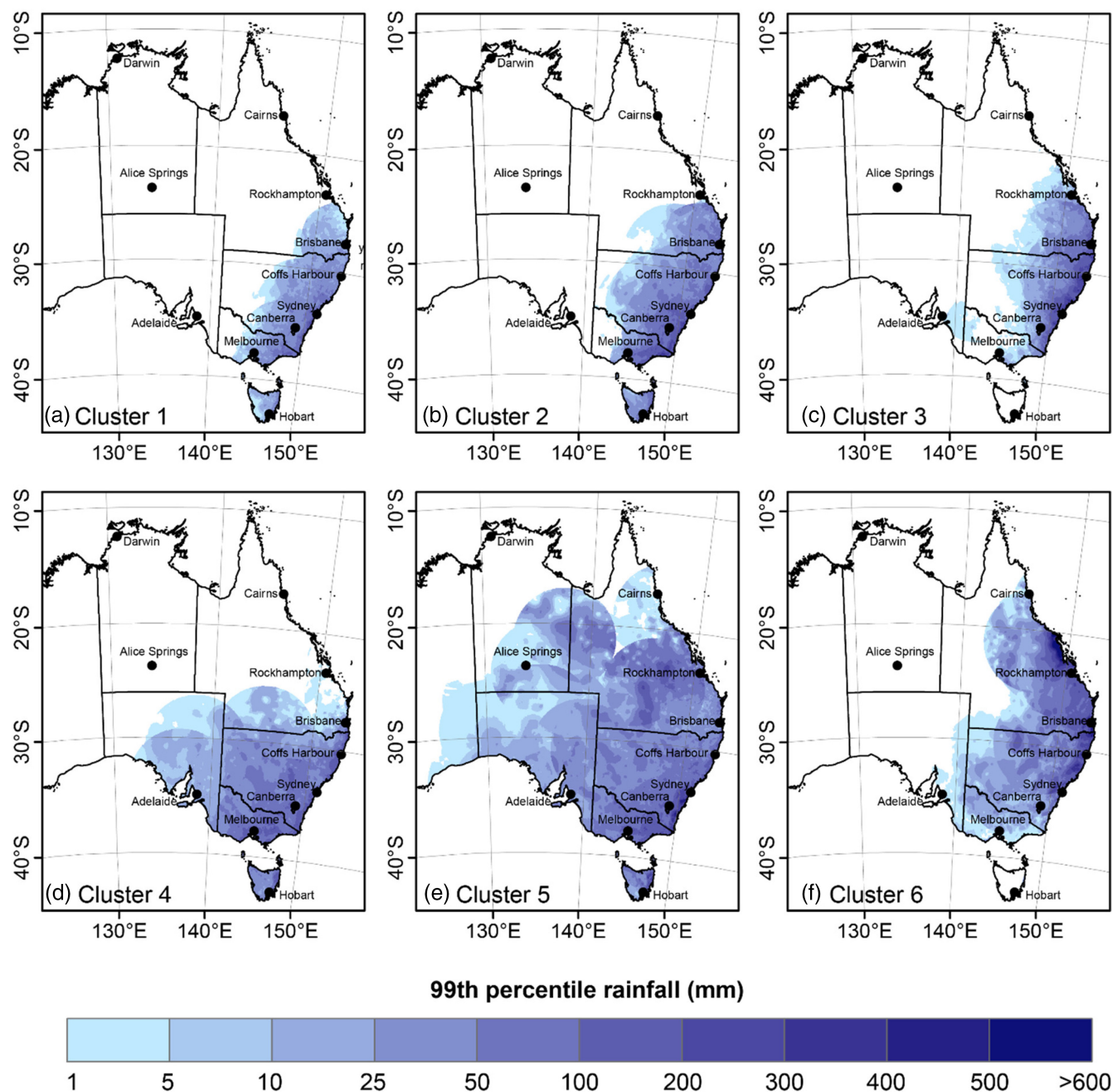


**FIGURE 7** The 99th percentile plots are used to determine areas impacted by extreme rainfall (mm) for each cluster. Areas of lower (higher) precipitation are highlighted in lighter (darker) colours. Plots are set out in consecutive order of cluster number. [Colour figure can be viewed at [wileyonlinelibrary.com](http://wileyonlinelibrary.com)]

IOD-positive months). Seasonally, the recurrence interval for C3 cyclones drops to approximately 7 months during IOD-positive JJA. For C4 and C5, cyclones during IOD-positive phases mostly occur between 1960 and 2000 (Figure S5D, E). Unlike C2 cyclones, C4 events are scarcer during IOD-negative winters (JJA), whereas SON storms are least likely during IOD-positive phases. Specifically, only three C6 ECCs were observed in JJA and none during SON (Table 1).

Teleconnections between SAM and ECCs are generally not statistically significant in this study (e.g. results present in Table S6). When compared to other climate drivers such as ENSO or the IOD, ECC frequency was significantly higher (lower) during positive and negative (neutral) SAM, particularly for C4 during SON. During SAM, the overall cyclone occurrence for all clusters except C3 is predominately in the positive phase (shown by the smallest recurrence

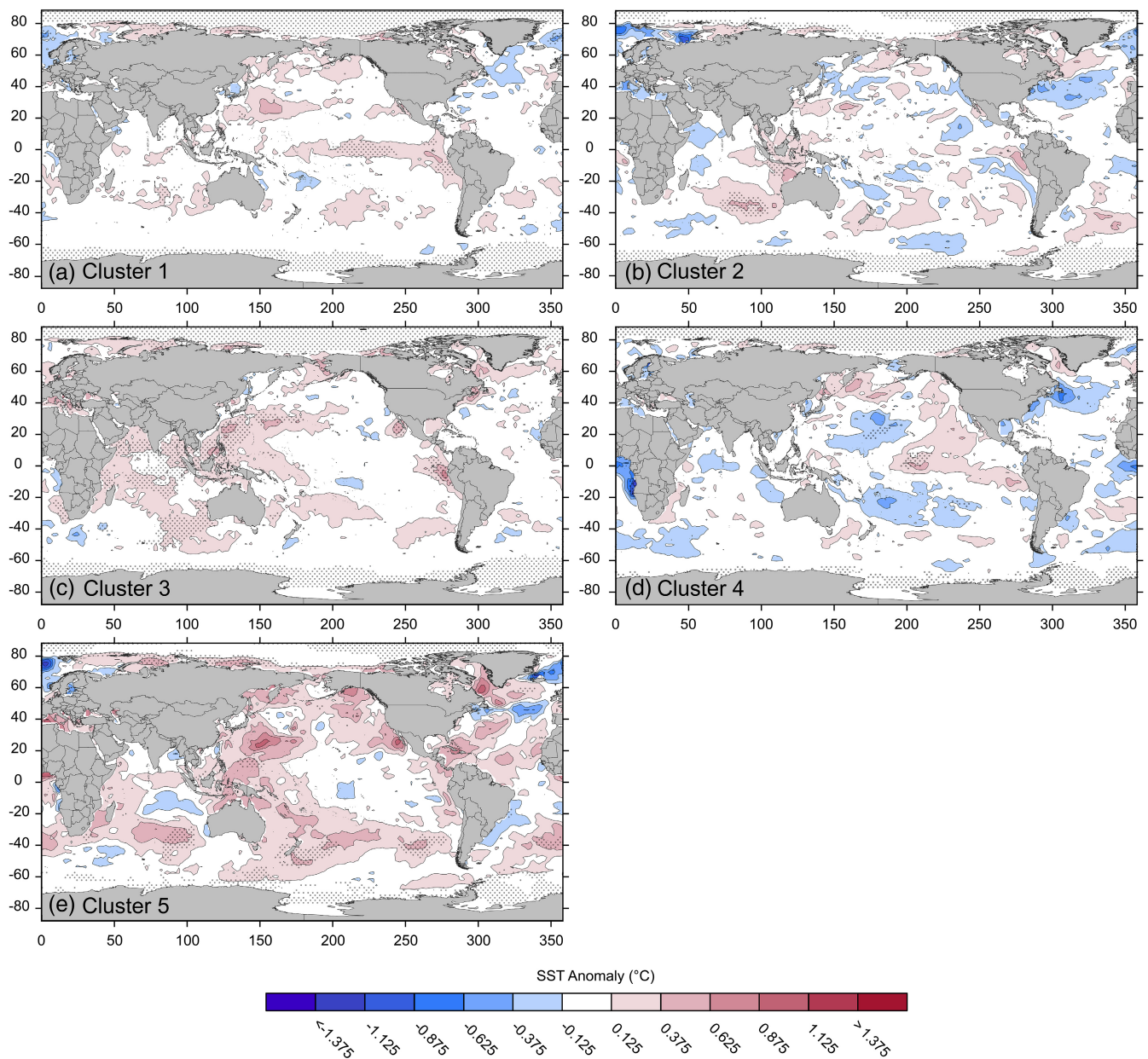


**FIGURE 8** Composite plots of SST (ERSSTv5) anomalies for each cluster based on the cluster median and genesis month for June, July and August. Regions of anomalously warmer or cooler SSTs are highlighted, along with areas of statistical significance (stippling) at a level of 0.01. Plots are set out in consecutive order of cluster, with a contour interval of 0.1. The ‘*stipple*’ and ‘*borders*’ functions from the Climate Data Toolbox for MATLAB (Greene et al., 2019) were used to create this figure. [Colour figure can be viewed at [wileyonlinelibrary.com](https://onlinelibrary.wiley.com/doi/10.1002/joc.8032)]

interval in Table 4; Figure S6). Significant differences for SAM-positive/-neutral combinations were present for all clusters except C6—and for the negative phases in C2 and C3. However, during JJA, none of the SAM phases were statistically dissimilar. Cyclones in C6 are mostly associated with the SAM-positive phase (Table 4; Figure S6). Because of the rarity (three events) of C6 storms in JJA and an absence in SON, this cluster has a limited relation (if any) to SAM in those seasons.

## 5 | DISCUSSION

This study aimed to identify the dominant track characteristics for each identified type of Australian ECC from 1950 to 2019 using cluster analysis. Seasonality and intensity were examined from the established clusters to determine any long-term trends or spatial patterns in their occurrence. Cyclones in each ECC cluster have a unique spatial signature of rainfall and impact on the Australian continent. Likewise, inferred broadscale conditions



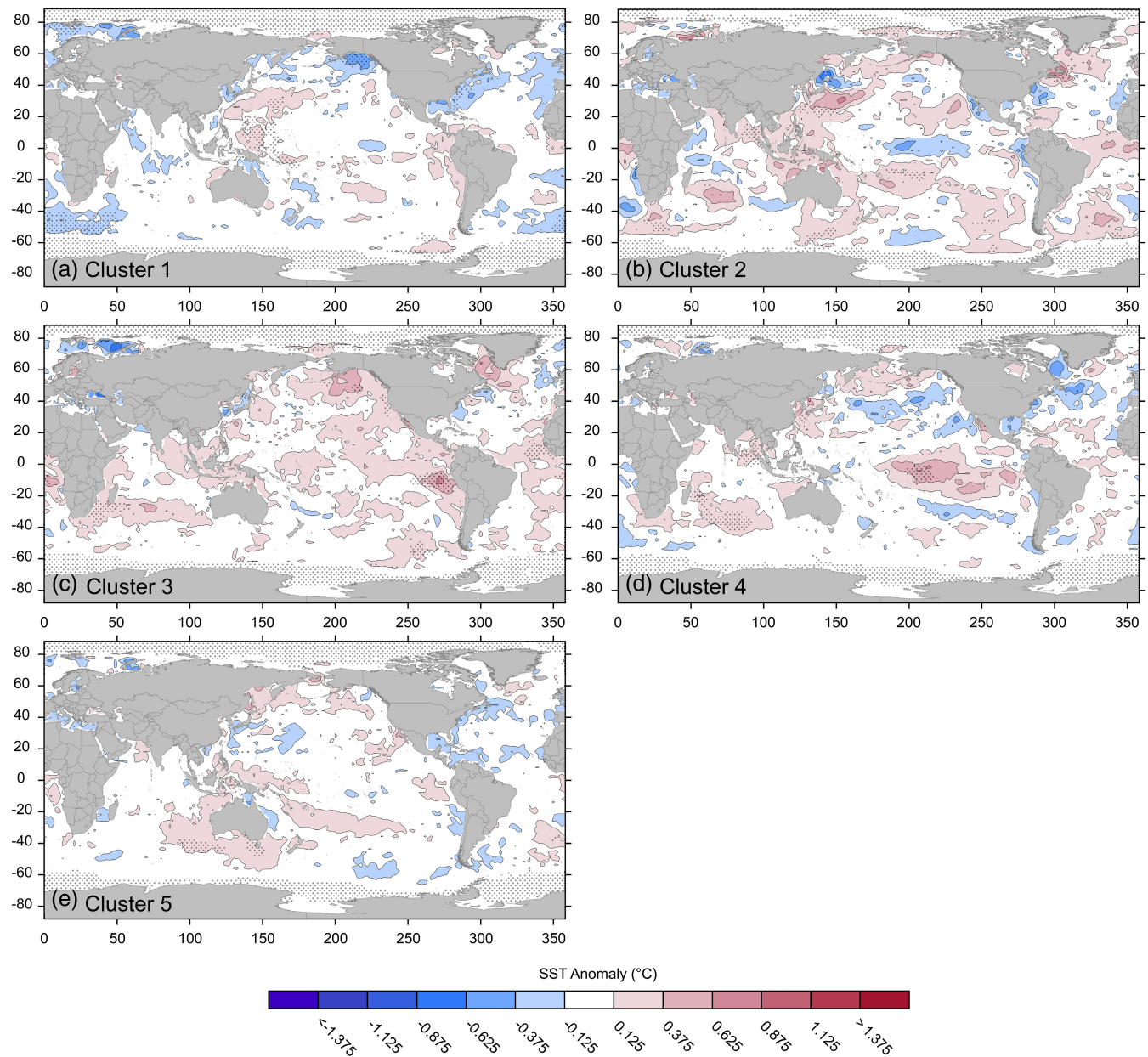


**FIGURE 9** Composite plots of SST (ERSSTv5) anomalies for each cluster based on the cluster median and genesis month for September, October and November. Regions of anomalously warmer or cooler SSTs are highlighted, along with areas of statistical significance (stippling) at a level of 0.01. Plots are set out in consecutive order of cluster, with a contour interval of 0.1. The ‘stipple’ and ‘borders’ functions from the Climate Data Toolbox for MATLAB (Greene et al., 2019) were used to create this figure. [Colour figure can be viewed at [wileyonlinelibrary.com](http://wileyonlinelibrary.com)]

(climate drivers) were linked with event incidence within the different ECC clusters.

Six statistically independent clusters were identified and further sub-classified into three groups based on ECC genesis location. Our detailed findings of the seasonality of ECC events within all clusters is generally consistent with previous research (Browning & Goodwin, 2013; Hopkins & Holland, 1997; Kiem et al., 2016; Speer et al., 2009). In particular, we show that ECCs are generated throughout the year, with a dominance of coastal

tracks (seen in C1, C2 and C3) during the austral winter months (June to August). Continental events (C4 and C5) are more prominent within the spring months (September to November), whereas tropical storms are mainly generated in summer (December to February). C3 was the only group of ECCs that displayed a significantly decreasing frequency over time (Figure 21). This cluster represents 27% of all storms from 1950 to 2019 (Table 1), with its mean track line positioned along the coastline tracking towards the QLD and NSW border.



**TABLE 3** The number of months in certain phases of ENSO, IOD and SAM from 1950 to 2019. These totals were used as  $n_1$  and  $n_2$  for the test of proportions.

	ENSO						IOD						SAM					
	Overall	JJA	SON	DJF	MAM	Overall	Overall	JJA	SON	DJF	MAM	Overall	Overall	JJA	SON	DJF	MAM	
Positive	231	50	60	65	56	279	78	85	51	65	267	65	65	65	69	73	60	
Negative	287	75	69	67	76	187	55	61	32	39	248	39	66	60	61	61	61	
Neutral	322	85	81	78	78	374	77	61	127	106	325	106	79	81	76	89	89	

Abbreviations: DJF, December January, February; JJA, June, July and August; MAM, March, April, May; SON, September, October, November.

Coastal tracks (C1, C2 and C3) were the more dominant type of ECCs, accounting for a combined total of 71% of all storms (Table 1). In contrast to previous studies (Browning & Goodwin, 2013, 2016; Speer et al., 2009), the characteristics of these tracks could be classified based on their location in proximity to the coastline. Compared to the definition by Browning and Goodwin (2013, 2016), tracks within coastal clusters align more closely to ETLs. Temporal trends in Browning and Goodwin (2013, 2016) do not align specifically with any particular cluster; however, Browning and Goodwin (2016) noted that the number of storm days decreased after 1955 (similar to C3). Conversely, if we consider the classifications of ECLs from Speer et al. (2009), coastal cyclones could be a combination of ETLs and ‘wave on a front low’. Tracks within these three clusters are shown to meander around the ECL box, predominately developing close to the coastline and travelling south/south-east towards the Pacific Ocean.

Continental lows (C4 and C5) have not previously been studied in as much detail, with many studies focusing primarily on the coastal lows. In our study, C4 tracks were centred around Tasmania and Victoria (i.e. the southern fraction of the ECL box). Many of these tracks are curved, with a southern origin and decay. Compared to the previous work of Browning and Goodwin (2013, 2016), these tracks/events are similar to SSLs. Furthermore, C4 cyclone characteristics resemble decaying frontal lows or ECL bomb events (Speer et al., 2009). The orientation of tracks in C5 is closely linked to westerlies and CLs (Browning & Goodwin, 2013, 2016; Speer et al., 2009). The majority of the genesis locations for storms in C5 are inland, on the western side of the Great Dividing Range. They then travel to the eastern seaboard. These systems have the highest intensity for all six clusters, maintaining their strength after reaching their MLAP value. This cluster also has the longest interaction time with land (averaging approximately 42 h). With respect to the tropical tracks represented by C6, they are closely related to previously identified tropical lows or ETCs (Browning & Goodwin, 2013, 2016; Speer et al., 2009)—based on their genesis location north of 30°S for most tracks, along with their seasonality (mainly summer occurrence) and intensity profile.

One of the most significant findings of this study is that the most intense storms and most widespread rainfall impacts are associated with the less studied continental lows (C4 and C5). Although less frequent, these systems deliver a vast quantity of rainfall quickly, making them a ‘high-risk’ system for extreme rainfall. Precipitation from C4 cyclones (75th and 99th percentiles) is delivered across Tasmania and Victoria and includes events such as the 1998 Sydney to Hobart Yacht Race. Land-

**TABLE 4** The overall observed recurrence interval (in months) of cyclones in positive (pos), negative (neg) and neutral (neu) phases of El Niño Southern Oscillation (ENSO), Indian Ocean Dipole (IOD) and Southern Annular Mode (SAM) for each cluster from 1950 to 2019. The recurrence interval (return period) is calculated using each phase's total number of months (presented in Table 3), divided by the total number of cyclone events that occurred in the corresponding phase for each cluster. Larger (smaller) values correlate to a lower (higher) frequency of cyclone events in the climate-specific phase. Positive and negative phases that are significantly different (at the level of 0.01) compared to the neutral state are highlighted in bold. The supplementary section (Table S6) presents the original statistical analysis and *p*-values linked to this table.

Overall	ENSO			IOD			SAM		
	Pos	Neg	Neu	Pos	Neg	Neu	Pos	Neg	Neu
1	4.9	<b>6.8</b>	3.7	<b>14.0</b>	<b>17.0</b>	2.6	<b>3.9</b>	4.4	6.4
2	<b>12.8</b>	11.5	6.9	<b>31.0</b>	<b>31.2</b>	5.0	<b>7.2</b>	<b>7.3</b>	17.1
3	<b>10.0</b>	<b>6.5</b>	3.4	<b>13.3</b>	<b>13.4</b>	2.9	<b>4.5</b>	<b>3.9</b>	8.3
4	10.0	13.7	8.5	<b>19.9</b>	<b>17.0</b>	6.6	<b>7.0</b>	9.9	17.1
5	17.8	19.1	10.4	<b>23.3</b>	<b>46.8</b>	8.7	<b>10.7</b>	12.4	23.2
6	57.8	23.9	24.8	<b>279.0</b>	<b>187.0</b>	13.9	22.3	41.3	29.6

based rainfall is spatially more extensive in C5 due to the length and coverage of the tracks. In the more extreme case (99th percentile), the affected areas are greater, with precipitation concentrated in central QLD, Victoria and southern NSW. This finding is significant because C5 cyclones can produce high rainfall over some of Australia's largest catchments. Compared to the smaller coastal catchments, those located west of the Great Dividing Range can produce significant floods with lower rainfall totals (due to the size of the drainage basin and topography; Jaffrés et al., 2021, 2022). These regions (e.g. the Murray-Darling Basin) are also important for Australia's food production—and extreme, spatially widespread rainfall can have a significant, negative effect on the economy of these regions, as well as displacing communities and affect infrastructure and transport (Dey et al., 2019; Dowdy et al., 2019; Ho et al., 2015; Westra et al., 2016).

In comparison to the infrequent but highly impactful continental lows, the coastal lows were found to deliver less rainfall over a much more restricted region. Indeed, the 50th percentile rainfall for C1 (the most common storm type) has no continental or land-based rainfall (Figure 5a), with most tracks remaining offshore. This pattern is attributable to the seaward movement of C1 tracks, resulting in little impact on land (lowest mean duration near the land of ~1.5 h; Table 1). Similarly, the 75th percentile displays minimal rainfall focused along the central coast of NSW. In the extreme case (99th percentile), C1 had minimal rainfall across the lower east coast, with areas of higher rainfall (>100 mm) aligned with the cluster genesis location. Median land-based rainfall (Figure 5) for C2 and C3 was slightly more prominent but still minimal. Areas of median rainfall are mostly

adjacent to cyclone genesis points, the storms generally delivering between 0 and 50 mm of rainfall. The 75th percentile illustrates a slightly more extensive spatial coverage for C2, with associated rainfall depths reaching up to 100 mm. In the 99th percentile, rainfall extends over four states for C2 and three for C3. C2 rainfall is more widespread, with higher values located around the NSW and Victorian border. In contrast, higher rainfall for C3 is heavily focused along the NSW coastline up into QLD. Again, C2 (~7 h) and C3 (~4.4 h) had relatively little interaction with the land (Table 1), which would contribute to the minimal rainfall quantity compared to the continental and tropical clusters. Finally, the least common cluster (C6)—representing tropical lows—also delivers extreme rainfall but to a more focused area centred around Brisbane. The highest rainfall amounts for the 75th and 99th percentiles extend this area of impact to the border between NSW and QLD. More extreme cases encompassed the coastline of central NSW to central QLD, the site of significant floods in 2022. Although infrequent, tropical lows are a concern to highly populated areas (i.e. Brisbane and northern NSW) due to their ability to deliver a large volume of rainfall in a very short period of time. In addition, tropical lows have the capacity to transition into ETCs, extending their impacts to more southern catchments (e.g. the June 2016 ECL event that transitioned from a low and combined with a king tide; Australian Bureau of Meteorology, 2016).

The seasonal breakdown of austral winter and spring SSTs for each cluster provides insight into a potential connection between ECC occurrence and large-scale climate drivers. For example, SST anomalies for C1 and C4 suggest that central Pacific El Niño conditions (Figure 8;

JJA	ENSO			IOD			SAM		
	Pos	Neg	Neu	Pos	Neg	Neu	Pos	Neg	Neu
1	4.17	4.69	2.93	<b>11.14</b>	<b>11.00</b>	1.71	3.25	3.00	5.27
2	12.50	15.00	5.31	<b>39.00</b>	<b>13.75</b>	4.05	8.13	8.25	8.78
3	<b>5.00</b>	<b>5.36</b>	2.02	<b>7.09</b>	<b>9.17</b>	1.57	3.25	2.54	3.95
4	6.25	<b>75.00</b>	6.07	8.67	27.50	6.42	7.22	11.00	9.88
5	50.00	15.00	12.14	<b>78.00</b>	<b>NA</b>	6.42	10.83	11.00	79.00
6	25.00	NA	85.00	78.00	NA	38.50	NA	33.00	79.00

Abbreviations: ENSO, El Niño Southern Oscillation; IOD, Indian Ocean Dipole; neg, negative; neu, neutral; pos, positive; SAM, Southern Annular Mode.

**TABLE 6** As per Table 4 but for September, October and November (SON). Original statistical analysis and *p*-values for this table are presented in Table S8.

SON	ENSO			IOD			SAM		
	Pos	Neg	Neu	Pos	Neg	Neu	Pos	Neg	Neu
1	4.62	5.31	3.52	<b>7.73</b>	<b>15.25</b>	1.88	3.29	5.00	5.06
2	12.00	11.50	10.13	<b>17.00</b>	<b>61.00</b>	4.92	8.63	7.50	27.00
3	15.00	6.90	8.10	<b>17.00</b>	<b>20.33</b>	4.00	6.90	7.50	13.50
4	6.67	6.90	8.10	<b>21.25</b>	<b>10.17</b>	3.37	<b>4.93</b>	<b>5.45</b>	20.25
5	7.50	11.50	5.40	7.73	<b>15.25</b>	4.57	5.75	8.57	8.10
6	NA	NA	NA	NA	NA	NA	NA	NA	NA

Abbreviations: ENSO, El Niño Southern Oscillation; IOD, Indian Ocean Dipole; neg, negative; neu, neutral; pos, positive; SAM, Southern Annular Mode.

Freund et al., 2021) might increase the likelihood of C1 and C4 storms. However, C1 events overall develop more frequently during ENSO-neutral conditions (Table 4). In addition, C3 events in the La Niña phase only occurred before 1979, with the greatest frequency of ECCs generated around the 1970s (Figure S4). This also corresponds to a period when La Niña events were more frequent (Meyers et al., 2007; Verdon, Wyatt, et al., 2004). Conversely, overall (Figure S2) and JJA (Figure S3) SST anomalies for C6 were suggestive of a weak La Niña and IOD-negative/-neutral (both climate conditions are conducive for increased rainfall for the Australian east coast). For most clusters, the composite SST anomaly patterns during spring were distinct from winter. Spring SSTs were characterised by generally cooler conditions for C1 and warmer-than-average conditions for C2, C3, C4 and C5. Anomalously warm winter SSTs are most distinct for C5, C6 and—to a lesser extent—C1 and C3, with cooler conditions relatively dominant in C4.

C6 winter SST anomalies are the most extreme for all clusters, with an SST signature characterised by strong anomalies globally, particularly warmer waters throughout the Indian Ocean and cooler conditions along the

east coast of Australia (Figure S3). These conditions coincide with IOD-neutral and La Niña/ENSO-neutral (Dowdy et al., 2019; Meyers et al., 2007; Risbey et al., 2009; Verdon et al., 2004; Verdon et al., 2004). Similar to C5, these background environmental conditions—alongside the extreme rainfall potential for C6 ECCs—mean that these storms have a high impact potential. However, signals within the SST plots could contain bias based on the limited number of events (smaller sample size when compared to C1 and C3), which could be evident in C5 and C6 (Figure 8). A more extensive rainfall signature (in terms of rainfall depth) noted for C5 and C6 can be attributed to the longer tracks and duration (Table 2) of events—along with an extensive period near/over land (Table 1). All three attributes create more opportunities to capture rainfall over that period.

Compared to the findings of Browning and Goodwin (2013, 2016), the nature of coastal cyclones (C1, C2, C3) and ETLs displayed both similarities and differences. Browning and Goodwin (2013, 2016) highlighted SST anomalies along the south coast of Australia and the western coastline (as seen in C3), whereas a warm signature was present in the central Pacific for the SST

**TABLE 5** As per Table 4 but for June, July and August (JJA). Values that are italicised convey a statistical difference between positive and negative phases. The supplementary section (Table S7) presents the original statistical analysis and *p*-values linked to this table.

analysis (as seen in C1). Dissimilarly to our results, cooler temperatures were recorded for the Australia north and east coast and the Indian Ocean (demonstrated in Browning & Goodwin, 2013, 2016), not matching our study's overall and seasonal results.

An important aspect of this study is the consideration of all three phases of each of the climate drivers within the analysis, with the neutral years producing the most unusual results. Hopkins and Holland (1997) suggested that the occurrence of ECCs was more frequent during transitional ENSO periods (e.g. the period when El Niño changes into La Niña). This could explain why we observed a majority of the ECCs forming during ENSO-neutral phases, often in the period between the two ENSO extremes. Cyclone formation within this study was predominantly associated with the IOD-neutral phase, highlighted by their significantly different recurrence intervals compared to the extreme IOD phases (Figure S5, Tables S6–S8). This indefinite relationship between the extreme IOD phases and ECC events is not unexpected, especially when considering Pepler, Timbal, et al. (2014).

During SAM-positive phases, all clusters except C3 have lower recurrence intervals and, thus, higher ECC frequency (Table 4). Furthermore, the tests of proportions highlighted a significant difference between the positive and neutral phases of SAM (excluding C6). However, ECC occurrences in negative and positive SAM were similar in most cases. The general absence in significance between cyclone prevalence and SAM phases was also reflected on a seasonal scale (Table 5 and Table 6). The chosen SAM index (KNMI Climate Explorer, 2022) may be a limitation of this analysis because it is not one of the conventional indices (Ho et al., 2012) chosen for climate-based studies. As Ho et al. (2012) discussed, the best choice of SAM index depends on the method, data source and time period (Ho et al., 2012; Marshall, 2003). This specific SAM index was used because it encompassed the entire time-period (1950 to 2019) of the study. Another difference compared with some studies is our choice of climatological baseline used to generate anomalies. Here, we used the long-term median over the entire period instead of the 30-year climatological mean recommended by the WMO. Initially, both baselines were adopted to compare SST results. After the detrending process, it was resolved that, in this case, the long-term median (1950–2019) was more representative than the 30-year climatological mean (1981–2010 or 1991–2020).

The relatively short period covered within this study limits the detection of long-term, decadal-scale trends. A longer instrumental record of ECC tracks that mirrors the historical documentation (and includes recent events) would provide a more robust analysis of temporal trends

and potentially more definite relationships with multi-decadal climate drivers (Gray et al., 2021). An ECC study covering a longer historical period could be explored using the 20th-century reanalysis ensemble (similar to Browning & Goodwin, 2016; Pepler et al., 2017). Thus, longer-term temporal changes in cyclone types corresponding to our clusters might not be present or easily identifiable based on the shorter period analysed here.

This study has a component of track bias from the pre-filtered dataset used for the clustering. Because we have restricted tracks based on their presence in the ECL box, this may have excluded relevant events (i.e. storms with land-based impact) outside the box (Gray et al., 2021). Future ECC studies could be improved by defining a new area or filtering processes inclusive of Tasmania and ITL systems that form within the Gulf of Carpentaria — comprising land-based areas of eastern Australia and not just the offshore region.

The precipitation database (SILO) used in this study restricted the analysis to land-based rainfall only. Future improvements to this study could adopt other precipitation databases (e.g. ERA5) that include an offshore rainfall signature. In addition, exploring sub-daily rainfall (instead of daily) or potential precipitable water could provide a more in-depth analysis of these events. Finally, analysis into wind, inundation and swells would provide useful insights for impact analysis on the different types of clusters—particularly C4 and C5.

Further analysis into continental clusters may be advantageous, although recent studies (Cavicchia et al., 2019; Di Luca et al., 2016; Dowdy, Mills, Timbal, & Wang, 2013; Dowdy et al., 2019; Pepler et al., 2016; Pepler and Dowdy, 2021b) suggest that the frequency of these and all other cyclones are expected to decrease in the future. In contrast, Speer et al. (2021) emphasise an upward trend for continental storms and, as found in this study, determined that these types of events may become more frequent in the future. It is clear that, as noted by Pepler and Dowdy (2021a), improved precipitation projections and a better understanding of the spatial extent of potential rainfall impacts of ECCs are needed—because these systems not only affect east coast communities but also inland Australia.

## 6 | CONCLUSION

In Australia, where rainfall variability is high and the pendulum commonly swings between extremes, improving our ability to predict, mitigate and manage cyclonic events is important across a range of sectors. This study contributes to the already large body of ECC knowledge by distinguishing and describing important characteristics of six



ECC clusters. We also identified three general groups of clusters based on their genesis location and track characteristics: coastal (C1, C2, C3), continental (C4, C5) and tropical (C6). The key finding of this study highlights that the more common types of cyclones (close orientation to the coast) are the least intense and have the least impactful rainfall and intensification. More intense ECCs were associated with storms generated over the continent (C5). These cyclones also had, on average, the greatest spatial extent of event rainfall than any other cluster. However, tropical (C6) events produce more rainfall, with precipitation primarily focused along the QLD and northern NSW coastline. Only C3 storms displayed a significant decrease in frequency after 1979, whereas all other ECC clusters show no long-term trend in their occurrence.

Seasonal SST anomalies during ECC events revealed conditions that appear to be conducive to cyclone generation. Localised areas of significantly warmer water in the southern Indian Ocean and central Pacific were associated with events in C1, C3, C5 and C6. The obtained signatures—particularly a positive SST anomaly in winter for C1 and in the spring for C4—suggest the potential influence of the central Pacific El Niño in storm genesis. Neutral ENSO, IOD-neutral and SAM-positive phases are dominant during the storm genesis of most clusters, a finding that suggests ECCs develop within transitional periods, generating fluctuations in localised conditions (Hopkins & Holland, 1997). This finding requires more research and an extended (or updated database) to yield potentially more significant results.

Understanding the seasonality and climate conditions that influence different classes of cyclones will aid in developing more accurate forecasts to improve the management of future ECC events. Expanding on this and other ECC work will improve the forecasting and database standards of ECCs to that of TCs (i.e. real-time). Furthermore, this study identified key characteristics of ECC events over the last 70 years. These could be used to determine potential changes in ECC occurrence in the future as climate continues to evolve with anthropogenic climate change. For example, high-resolution, downscaled pressure data from global climate models could be used to establish the relative change in the prevalence of the six ECC clusters. Given the range and severity of the different clusters, this information is crucial to ensure that our regions and cities are prepared for any increased risk of rainfall extremes in the coming decades.

#### AUTHOR CONTRIBUTIONS

**Jessie L. Gray:** Conceptualization; methodology; visualization; writing – review and editing; writing – original

draft; investigation; formal analysis; software; project administration; resources. **Danielle C. Verdon-Kidd:** Resources; supervision; conceptualization; methodology; formal analysis; funding acquisition; validation; writing – review and editing; visualization; investigation. **Jasmine B. D. Jaffrés:** Formal analysis; investigation; software; methodology; supervision; visualization; writing – review and editing; conceptualization; validation. **Michael G. Hewson:** Conceptualization; formal analysis; methodology; validation; visualization; writing – review and editing; supervision; investigation. **John M. Clarke:** Funding acquisition; supervision; writing – review and editing; validation. **Krishneel K. Sharma:** Methodology; software; validation; writing – review and editing. **Nathan B. English:** Conceptualization; methodology; funding acquisition; visualization; writing – review and editing.

#### ACKNOWLEDGEMENTS

Jessie L. Gray acknowledges the financial support of Central Queensland University (CQU), financial support from a postgraduate scholarship from the Commonwealth Scientific and Industrial Research Organization (CSIRO, John Clarke supervising) and C&R Consulting. The authors would like to acknowledge Jason Bell and the CQUniversity HPC computing facility for computation and programming assistance. Finally, the authors would like to acknowledge the First Nations Peoples, the Bindal and Wulgurukaba, of the land this research was conducted on and we also pay our respect to their elder's past, present and emerging. Open access publishing facilitated by Central Queensland University, as part of the Wiley - Central Queensland University agreement via the Council of Australian University Librarians.

Toolboxes and data were sourced from the following sites: CCToolbox: <http://www.datalab.uci.edu/software/CCT/#Down>; Climate Data Toolbox for MATLAB: [http://www.chadagreene.com/CDT/CDT\\_Content.html](http://www.chadagreene.com/CDT/CDT_Content.html); SILO database: <https://www.longpaddock.qld.gov.au/silo/gridded-data/>; ERSSTv5 Niño 3.4 index: <https://climexp.knmi.nl/data/iersstnino3.4a.dat>; DMI: <https://climexp.knmi.nl/data/idmiersst.dat>; SAM: [http://climexp.knmi.nl/data/isam\\_ncepncar.dat](http://climexp.knmi.nl/data/isam_ncepncar.dat); SST: <https://climexp.knmi.nl/select.cgi?id=someone@somewhere&field=ersstv5>; Raw cyclone data (NCEP1; Pepler, 2020a): [https://figshare.com/collections/Australian\\_region\\_cyclones\\_1950-2019/4944135/1](https://figshare.com/collections/Australian_region_cyclones_1950-2019/4944135/1).

#### ORCID

Jessie L. Gray  <https://orcid.org/0000-0002-4797-7682>

Danielle C. Verdon-Kidd  <https://orcid.org/0000-0001-5334-4251>

Jasmine B. D. Jaffrés  <https://orcid.org/0000-0003-2567-539X>

Michael G. Hewson  <https://orcid.org/0000-0002-5212-3921>

John M. Clarke  <https://orcid.org/0000-0003-1894-0378>

Krishneel K. Sharma  <https://orcid.org/0000-0001-6802-2239>

Nathan B. English  <https://orcid.org/0000-0002-6936-8079>

## REFERENCES

- Australian Bureau of Meteorology. 2016. *Special climate statement 57 —extensive early June rainfall affecting the Australian east coast*. Melbourne: Bureau of Meteorology.
- Australian Bureau of Meteorology. (2022) About ENSO and IOD indices.
- Australian Institute for Disaster Resilience. (2020) Sydney to Hobart Yacht Race, 1998.
- Browning, S. & Goodwin, I. (2016) Large-scale drivers of Australian east coast cyclones since 1851. *Journal of Southern Hemisphere Earth System Science*, 66(2), 125–151. Available from: <https://doi.org/10.22499/3.6602.004>
- Browning, S.A. & Goodwin, I.D. (2013) Large-scale influences on the evolution of winter subtropical maritime cyclones affecting Australia's east coast. *Monthly Weather Review*, 141(7), 2416–2431. Available from: <https://doi.org/10.1175/MWR-D-12-00312.1>
- Buckley, B.W. & Leslie, L.M. (2000) The Australian boxing day storm of 1998 - synoptic description and numerical simulations. *Weather and Forecasting*, 15(5), 543–558. Available from: [https://doi.org/10.1175/1520-0434\(2000\)015<0543:TABDSO>2.0.CO;2](https://doi.org/10.1175/1520-0434(2000)015<0543:TABDSO>2.0.CO;2)
- Camargo, S.J., Robertson, A.W., Barnston, A.G. & Ghil, M. (2008) Clustering of eastern North Pacific tropical cyclone tracks: ENSO and MJO effects. *Geochemistry, Geophysics, Geosystems*, 9(6), 1–23. Available from: <https://doi.org/10.1029/2007GC001861>
- Catto, J.L. (2018) A new method to objectively classify extratropical cyclones for climate studies: testing in the Southwest Pacific region. *Journal of Climate*, 31(12), 4683–4704. Available from: <https://doi.org/10.1175/JCLI-D-17-0746.1>
- Cavicchia, L., Dowdy, A. & Walsh, K. (2018) Energetics and dynamics of subtropical Australian east coast cyclones: two contrasting cases. *Monthly Weather Review*, 146(5), 1511–1525. Available from: <https://doi.org/10.1175/MWR-D-17-0316.1>
- Cavicchia, L., Pepler, A., Dowdy, A. & Walsh, K. (2019) A physically based climatology of the occurrence and intensification of Australian east coast lows. *Journal of Climate*, 32(10), 2823–2841. Available from: <https://doi.org/10.1175/JCLI-D-18-0549.1>
- Chiew, F. & Siriwardena, L. (2005) *Trend/change detection software: user manual, eWater toolkit: documentation*. Australia: University of Melbourne, pp. 1–29.
- Corporal-Lodangco, I.L., Richman, M.B., Leslie, L.M. & Lamb, P.J. (2014) Cluster analysis of North Atlantic tropical cyclones. *Procedia Computer Science*, 36(C), 293–300. Available from: <https://doi.org/10.1016/j.procs.2014.09.096>
- Dacre HF, Pinto JG. 2020. Serial clustering of extratropical cyclones: a review of where, when and why it occurs. *Npj Climate and Atmospheric Science*. 3(1): 1–10. <https://doi.org/10.1038/s41612-020-00152-9>.
- Dey, R., Lewis, S.C., Arblaster, J.M. & Abram, N.J. (2019) A review of past and projected changes in Australia's rainfall. *Wiley Interdisciplinary Reviews: Climate Change*, 10(3), 1–23. Available from: <https://doi.org/10.1002/wcc.577>
- Di Luca, A., Evans, J., Pepler, A., Alexander, L., & Argüeso, D. (2016). Evaluating the representation of Australian East Coast Lows in a regional climate model ensemble. *Journal of Southern Hemisphere Earth System Science*. Bureau of Meteorology, Australia, 66(2), 108–124. <https://doi.org/10.22499/3.6602.003>
- Dowdy, A.J., Mills, G.A. & Timbal, B. (2013) Large-scale diagnostics of extratropical cyclogenesis in eastern Australia. *International Journal of Climatology*, 33(10), 2318–2327. Available from: <https://doi.org/10.1002/joc.3599>
- Dowdy, A.J., Mills, G.A., Timbal, B. & Wang, Y. (2013) Changes in the risk of extratropical cyclones in eastern Australia. *Journal of Climate*, 26(4), 1403–1417. Available from: <https://doi.org/10.1175/JCLI-D-12-00192.1>
- Dowdy, A.J., Pepler, A., Di Luca, A., Cavicchia, L., Mills, G., Evans, J.P. et al. (2019) Review of Australian east coast low pressure systems and associated extremes. *Climate Dynamics*, 53(7–8), 4887–4910. Available from: <https://doi.org/10.1007/s00382-019-04836-8>
- Freund, M.B., Marshall, A.G., Wheeler, M.C. & Brown, J.N. (2021) Central Pacific El Niño as a precursor to summer drought-breaking rainfall over southeastern Australia. *Geophysical Research Letters*, 48(7), 1–9. Available from: <https://doi.org/10.1029/2020GL091131>
- Gaffney, S. (2004) *Probabilistic curve-aligned clustering and prediction with regression mixture models*. Irvine: University of California.
- Gaffney, S.J., Robertson, A.W., Smyth, P., Camargo, S.J. & Ghil, M. (2007) Probabilistic clustering of extratropical cyclones using regression mixture models. *Climate Dynamics*, 29(4), 423–440. Available from: <https://doi.org/10.1007/s00382-007-0235-z>
- Gray, J.L., Jaffrés, J.B.D., Verdon-Kidd, D.C., Hewson, M.G., Clarke, J.M., Pepler, A. et al. (2021) A comparison of the MATCHES and NCEP1 databases for use in Australian east coast low studies. *Weather and Climate Extremes*, 34, 1–16. Available from: <https://doi.org/10.1016/j.wace.2021.100400>
- Gray, J.L., Verdon-Kidd, D.C., Callaghan, J.C. & English, N.B.A. (2020) On the recent hiatus of tropical cyclones landfalling in NSW, Australia. *Journal of Southern Hemisphere Earth System Science*, 70(1), 1–13.
- Greene, C.A., Thirumalai, K., Kearney, K.A., Delgado, J.M., Schwanghart, W., Wolfenbarger, N.S. et al. (2019) The climate data toolbox for MATLAB. *Geochemistry, Geophysics, Geosystems*, 20(7), 3774–3781. Available from: <https://doi.org/10.1029/2019GC008392>
- Greenslade, D.J.M. (2001) A wave modelling study of the 1998 Sydney to Hobart Yacht Race. *Australian Meteorological Magazine*, 50(1), 53–63.
- Ho, M., Kiem, A. & Verdon-Kidd, D.C. (2015) A paleoclimate rainfall reconstruction in the Murray-Darling basin (MDB), Australia: 1. Evaluation of different paleoclimate archives, rainfall networks, and reconstruction techniques. *Water Resources*

- Research, 51, 8362–8379. Available from: <https://doi.org/10.1111/j.1752-1688.1969.tb04897.x>
- Ho, M., Kiem, A.S. & Verdon-Kidd, D.C. (2012) The southern annular mode: a comparison of indices. *Hydrology and Earth System Sciences*, 16(3), 967–982. Available from: <https://doi.org/10.5194/hess-16-967-2012>
- Hogg, R. & Tanis, E. (1988) *Probability and statistical inference*. New York: Macmillan Publishing.
- Holland, G. (1997) The east coast cyclone. In: Webb, E.K. (Ed.) *Windows in meteorology: Australian perspective*. Collingwood: CSIRO Publishing, pp. 242–245.
- Hopkins, L.C. & Holland, G.J. (1997) Australian heavy-rain days and associated east coast cyclones: 1958–92. *Journal of Climate*, 10(4), 621–634. Available from: [https://doi.org/10.1175/1520-0442\(1997\)0102.0.CO;2](https://doi.org/10.1175/1520-0442(1997)0102.0.CO;2)
- Huang, B., Thorne, P.W., Banzon, V.F., Boyer, T., Chepurin, G., Lawrimore, J.H. et al. (2017) Extended reconstructed sea surface temperature, version 5 (ERSSTv5): upgrades, validations, and intercomparisons. *Journal of Climate*, 30(20), 8179–8205. Available from: <https://doi.org/10.1175/JCLI-D-16-0836.1>
- Jaffrés, J.B.D., Cuff, B., Cuff, C., Faichney, I., Knott, M. & Rasmussen, C. (2021) Hydrological characteristics of Australia: relationship between surface flow, climate and intrinsic catchment properties. *Journal of Hydrology*, 603(April), 126911. Available from: <https://doi.org/10.1016/j.jhydrol.2021.126911>
- Jaffrés, J.B.D., Cuff, B., Cuff, C., Knott, M. & Rasmussen, C. (2022) Hydrological characteristics of Australia: national catchment classification and regional relationships. *Journal of Hydrology*, 612, 127969. Available from: <https://doi.org/10.1016/j.jhydrol.2022.127969>
- Jaffrés J.B.D. & Gray J.L. 2023. *Chasing rainfall: estimating event precipitation along tracks of tropical cyclones via reanalysis data and in-situ gauges*. Townsville: C&R Consulting.
- Jeffrey, S.J., Carter, J.O., Moodie, K.B. & Beswick, A.R. (2001) Using spatial interpolation to construct a comprehensive archive of Australian climate data. *Environmental Modelling and Software*, 16(4), 309–330. Available from: [https://doi.org/10.1016/S1364-8152\(01\)00008-1](https://doi.org/10.1016/S1364-8152(01)00008-1)
- Ji, F., Pepler, A.S., Browning, S., Evans, J.P. & Di Luca, A. (2018) Trends and low frequency variability of East Coast lows in the twentieth century. *Journal of Southern Hemisphere Earth Systems Science*, 68(1), 1–15. Available from: <https://doi.org/10.22499/3.6801.001>
- Kalnay, E., Kanamitsu, M., Kistler, R., Collins, W., Deaven, D., Gandin, L. et al. (1996) The NCEP/NCAR 40-year reanalysis project. *Bulletin of the American Meteorological Society*, 77(3), 437–472.
- Kiem, A., Twomey, C., Lockart, N., Willgoose, G., Kuczera, G., Chowdhury, A.K. et al. (2016) Links between East Coast lows and the spatial and temporal variability of rainfall along the eastern seaboard of Australia. *Journal of Southern Hemisphere Earth System Science*, 66(2), 162–176. Available from: <https://doi.org/10.22499/3.6602.006>
- Kim, H.S., Kim, J.H., Ho, C.H. & Chu, P.S. (2011) Pattern classification of typhoon tracks using the fuzzy c-means clustering method. *Journal of Climate*, 24(2), 488–508. Available from: <https://doi.org/10.1175/2010JCLI3751.1>
- Kirkland, J.L. & Zick, S.E. (2019) Regional differences in the spatial patterns of North Atlantic tropical cyclone rainbands through landfall. *Southeastern Geographer*, 59(3), 294–320. Available from: <https://doi.org/10.1353/sgo.2019.0023>
- KNMI Climate Explorer. (2022) Time Series: Monthly SAM NCEP/NCAR.
- Kossin, J.P., Camargo, S.J. & Sitkowski, M. (2010) Climate modulation of North Atlantic hurricane tracks. *Journal of Climate*, 23(11), 3057–3076. Available from: <https://doi.org/10.1175/2010JCLI3497.1>
- Lim, E.P. & Simmonds, I. (2007) Southern hemisphere winter extratropical cyclone characteristics and vertical organization observed with the ERA-40 data in 1979–2001. *Journal of Climate*, 20(11), 2675–2690. Available from: <https://doi.org/10.1175/JCLI4135.1>
- Mailier, P.J., Stephenson, D.B., Ferro, C.A.T. & Hodges, K.I. (2006) Serial clustering of extratropical cyclones. *Monthly Weather Review*, 134(8), 2224–2240. Available from: <https://doi.org/10.1175/MWR3160.1>
- Marshall, G.J. (2003) Trends in the Southern Annular Mode from observations and reanalyses. *Journal of Climate*, 16(24), 4134–4143. Available from: [https://doi.org/10.1175/1520-0442\(2003\)016<4134:TITSAM>2.0.CO;2](https://doi.org/10.1175/1520-0442(2003)016<4134:TITSAM>2.0.CO;2)
- McBride, J.L. & Holland, G.J. (1987) Tropical-cyclone forecasting: a worldwide summary of techniques and verification statistics. *Bulletin of the American Meteorological Society*, 68(10, Oct. 1987), 1230–1238. Available from: [https://doi.org/10.1175/1520-0477\(1987\)068<1230:tcfaws>2.0.co;2](https://doi.org/10.1175/1520-0477(1987)068<1230:tcfaws>2.0.co;2)
- Meyers, G., McIntosh, P., Pigot, L. & Pook, M. (2007) The years of El Niño, La Niña and interactions with the tropical Indian Ocean. *Journal of Climate*, 20(13), 2872–2880. Available from: <https://doi.org/10.1175/JCLI4152.1>
- Mills, G.A. (2001) Mesoscale cyclogenesis in reversed shear—the 1998 Sydney to Hobart yacht race storm. *Australian Meteorological Magazine*, 50(1), 29–52.
- Mortlock T, Somerville P. 2020. *February 2020 East Coast low: Sydney impacts*. St Leonards: SydneyRisk Frontiers.
- Mumby, P.J., Vitolo, R. & Stephenson, D.B. (2011) Temporal clustering of tropical cyclones and its ecosystem impacts. *Proceedings of the National Academy of Sciences of the United States of America*, 108(43), 17626–17630. Available from: <https://doi.org/10.1073/pnas.1100436108>
- Murray, R.J. & Simmonds, I. (1991) A numerical scheme for tracking cyclone centres from digital data. Part II: application to January and July general circulation model simulations. *Australian Meteorological Magazine*, 39(3), 167–180.
- Nakamura, J., Lall, U., Kushnir, Y. & Camargo, S.J. (2009) Classifying North Atlantic tropical cyclone tracks by mass moments. *Journal of Climate*, 22(20), 5481–5494. Available from: <https://doi.org/10.1175/2009JCLI2828.1>
- Nath, S., Kotal, S.D. & Kundu, P.K. (2015) Application of fuzzy clustering technique for analysis of North Indian Ocean tropical cyclone tracks. *Tropical Cyclone Research and Review*, 4(3–4), 110–123. Available from: <https://doi.org/10.6057/2015TCRRh3.02>
- National centers for environmental information (NOAA). (2022) *Equatorial Pacific Sea Surface Temperatures (SST)*. Boulder, CO: NOAA.
- Pepler, A. (2020a) Australian region cyclones, 1950–2019. figshare. Collection. <https://doi.org/10.6084/m9.figshare.c.4944135.v1>



- Pepler, A. (2020b) Record lack of cyclones in southern Australia during 2019. *Geophysical Research Letters*, 47(13), 1–9. Available from: <https://doi.org/10.1029/2020GL088488>
- Pepler, A., Coutts-Smith, A. & Timbal, B. (2014) The role of East Coast lows on rainfall patterns and inter-annual variability across the East Coast of Australia. *International Journal of Climatology*, 34(4), 1011–1021. Available from: <https://doi.org/10.1002/joc.3741>
- Pepler, A., & Dowdy A. (2021a). Intense east coast lows and associated rainfall in eastern Australia. *Journal of Southern Hemisphere Earth System Science*, 71, 110–122.
- Pepler, A., & Dowdy, A. (2021b). Fewer deep cyclones projected for the midlatitudes in a warming climate, but with more intense rainfall. *Environmental Research Letters*, 16(5). <https://doi.org/10.1088/1748-9326/abf528>.
- Pepler, A., Timbal, B., Rakich, C. & Coutts-Smith, A. (2014) Indian Ocean dipole overrides ENSO's influence on cool season rainfall across the eastern seaboard of Australia. *Journal of Climate*, 27, 3816–3826. Available from: <https://doi.org/10.1175/JCLI-D-13-00554.1>
- Pepler, A.S., Di Luca, A. & Evans, J.P. (2018) Independently assessing the representation of midlatitude cyclones in high-resolution reanalyses using satellite observed winds. *International Journal of Climatology*, 38(3), 1314–1327. Available from: <https://doi.org/10.1002/joc.5245>
- Pepler, A.S., Di Luca, A., Ji, F., Alexander, L.V., Evans, J.P. & Sherwood, S.C. (2015) Impact of identification method on the inferred characteristics and variability of Australian East Coast lows. *Monthly Weather Review. American Meteorological Society*, 143(3), 864–877. Available from: <https://doi.org/10.1175/mwr-d-14-00188.1>
- Pepler, A.S., Fong, J. & Alexander, L.V. (2017) Australian east coast mid-latitude cyclones in the 20th century reanalysis ensemble. *International Journal of Climatology*, 37(4), 2187–2192. Available from: <https://doi.org/10.1002/joc.4812>
- Pepler, A.S., Imielska, A., Coutts-Smith, A., Gamble, F. & Schweitzer, M. (2016) Identifying East Coast lows with climate hazards on the eastern seaboard. *Journal of Southern Hemisphere Earth Systems Science*, 66(2), 97–107.
- PERILS. (2020) *AUD 958M- PERILS releases detailed industry loss footprint for the February 2020 Australian east coast low*. Zurich.
- Pinto, J.G., Bellenbaum, N., Karremann, M.K. & Della-Marta, P.M. (2013) Serial clustering of extratropical cyclones over the North Atlantic and Europe under recent and future climate conditions. *Journal of Geophysical Research Atmospheres*, 118(22), 12,476–12,485. Available from: <https://doi.org/10.1002/2013JD020564>
- Pinto, J.G., Gomara, I., Masato, G., Dacre, H.F., Woollings, T. & Caballero, R. (2014) Large-scale dynamics associated with clustering of extratropical cyclones affecting Western Europe. *Journal of Geophysical Research: Atmospheres*, 119, 8410–8421. Available from: <https://doi.org/10.1002/2014JD022305>.  
Received
- Priestley, M.D.K., Pinto, J.G., Dacre, H.F. & Shaffrey, L.C. (2017) Rossby wave breaking, the upper level jet, and serial clustering of extratropical cyclones in western Europe. *Geophysical Research Letters*, 44(1), 514–521. Available from: <https://doi.org/10.1002/2016GL071277>
- Quinting, J.F., Catto, J.L. & Reeder, M.J. (2019a) Synoptic climatology of hybrid cyclones in the Australian region. *Quarterly Journal of the Royal Meteorological Society*, 145(718), 288–302. Available from: <https://doi.org/10.1002/qj.3431>
- Quinting, J.F., Reeder, M.J. & Catto, J.L. (2019b) The intensity and motion of hybrid cyclones in the Australian region in a composite potential vorticity framework. *Quarterly Journal of the Royal Meteorological Society*, 145(718), 273–287. Available from: <https://doi.org/10.1002/qj.3430>
- Rahman, M.S., Yang, R. & Di, L. (2018) Clustering Indian Ocean tropical cyclone tracks by the standard deviational ellipse. *Climate*, 6(2), 1–26. Available from: <https://doi.org/10.3390/cli6020039>
- Ramsay, H.A., Camargo, S.J. & Kim, D. (2012) Cluster analysis of tropical cyclone tracks in the southern hemisphere. *Climate Dynamics*, 39(3), 897–917. Available from: <https://doi.org/10.1007/s00382-011-1225-8>
- Risbey, J.S., Pook, M.J., McIntosh, P.C., Wheeler, M.C. & Hendon, H.H. (2009) On the remote drivers of rainfall variability in Australia. *Monthly Weather Review. American Meteorological Society*, 137(10), 3233–3253. Available from: <https://doi.org/10.1175/2009mwr2861.1>
- Sharma, K.K., Magee, A.D. & Verdon-Kidd, D.C. (2021) Variability of Southwest Pacific tropical cyclone track geometry over the last 70 years. *International Journal of Climatology*, 41(1), 529–546. Available from: <https://doi.org/10.1002/joc.6636>
- Simmonds, I., Murray, R.J. & Leighton, R.M. (1999) A refinement of cyclone tracking methods with data from FROST. *Australian Meteorological Magazine*, 48, 35–49.
- Speer, M., Leslie, L., Hartigan, J. & Macnamara, S. (2021) Changes in frequency and location of east coast low pressure systems affecting Southeast Australia. *Climate*, 9(3), 1–21. Available from: <https://doi.org/10.3390/cli9030044>
- Speer, M.S., Wiles, P. & Pepler, A. (2009) Low pressure systems off the New South Wales coast and associated hazardous weather: establishment of a database. *Australian Meteorological and Oceanographic Journal*, 58(1), 29–39. Available from: <https://doi.org/10.22499/2.5801.004>
- Verdon-Kidd, D. C. (2018). On the classification of different flavours of Indian Ocean Dipole events. *International Journal of Climatology*, 38(13), 4924–4937. <https://doi.org/10.1002/joc.5707>
- Verdon, D.C., Kiem, A.S. & Franks, S.W. (2004) Multi-decadal variability of forest fire risk - eastern Australia. *International Journal of Wildland Fire*, 13(2), 165–171. Available from: <https://doi.org/10.1071/WF03034>
- Verdon, D.C., Wyatt, A.M., Kiem, A.S. & Franks, S.W. (2004) Multi-decadal variability of rainfall and streamflow: eastern Australia. *Water Resources Research*, 40(10), 1–8. Available from: <https://doi.org/10.1029/2004WR003234>
- Verdon-Kidd, D., Kiem, A. & Willgoose, G. (2016) East coast lows and the pasha bulker storm - lessons learned nine years on. *Journal of Southern Hemisphere Earth System Science. Bureau of Meteorology, Australia*, 66(2), 152–161. Available from: <https://doi.org/10.22499/3.6602.005>
- Verdon-Kidd, D., Kiem, A., Willgoose, G. & Haines, P. (2010) East Coast lows and the Newcastle/central coast pasha bulker storm. *Gold Coast*, 61, 1–61.



- Warren, J.; Gilbert, R.O. (1988) Statistical methods for environmental pollution monitoring. *Technometrics*, 30, 348.
- Weaver, K.F., Morales, V.C., Dunn, S.L., Godde, K. & Weaver, P. (2018) *An introduction to statistical analysis in research : with applications in the biological and life sciences*. Hoboken: Wiley.
- Westra, S., White, C.J. & Kiem, A.S. (2016) Introduction to the special issue: historical and projected climatic changes to Australian natural hazards. *Climatic Change*, 139(1), 1–19. Available from: <https://doi.org/10.1007/s10584-016-1826-7>
- Wolff, N.H., Wong, A., Vitolo, R., Stolberg, K., Anthony, K.R.N. & Mumby, P.J. (2016) Temporal clustering of tropical cyclones on the great barrier reef and its ecological importance. *Coral Reefs*, 35(2), 613–623. Available from: <https://doi.org/10.1007/s00338-016-1400-9>
- Yu, J.H., Zheng, Y.Q., Wu, Q.S., Lin, J.G. & Bin, G.Z. (2017) K-means clustering for classification of the northwestern Pacific tropical cyclone tracks. *Journal of Tropical Meteorology*, 22(2), 127–135. Available from: <https://doi.org/10.16555/j.1006-8775.2016.02.003>

- Zheng, M., Chang, E.K.M., Colle, B.A., Luo, Y. & Zhu, Y. (2017) Applying fuzzy clustering to a multimodel ensemble for U.S. East Coast winter storms: scenario identification and forecast verification. *Weather and Forecasting*, 32(3), 881–903. Available from: <https://doi.org/10.1175/WAF-D-16-0112.1>

## SUPPORTING INFORMATION

Additional supporting information can be found online in the Supporting Information section at the end of this article.

**How to cite this article:** Gray, J. L., Verdon-Kidd, D. C., Jaffrés, J. B. D., Hewson, M. G., Clarke, J. M., Sharma, K. K., & English, N. B. (2023). Characterizing Australia's east coast cyclones (1950–2019). *International Journal of Climatology*, 43(7), 3324–3352. <https://doi.org/10.1002/joc.8032>